Department of Energy Technology

# Matching analysis for on-site building energy systems involving energy conversion, storage and hybrid grid connections

Sunliang Cao

Aalto University

DOCTORAL DISSERTATIONS

Sunliang Cao

Matching analysis for on-site building energy systems involving energy conversion, storage and hybrid grid connections

Aalto University

Aalto University publication series
**DOCTORAL DISSERTATIONS** 18/2014

# Matching analysis for on-site building energy systems involving energy conversion, storage and hybrid grid connections

**Sunliang Cao**

A doctoral dissertation completed for the degree of Doctor of Science (Technology) (Doctor of Philosophy) to be defended, with the permission of the Aalto University School of Engineering, at a public examination held at the lecture hall 172 in K4 building of the school on 28th March 2014 at 12.

**Aalto University**
**School of Engineering**
**Department of Energy Technology**
**Building Energy Efficiency and HVAC-Technology**

**Supervising professor**
Professor Kai Sirén, Aalto University, Finland.

**Thesis advisor**
Dr. Ala Hasan, Technical Research Centre of Finland VTT, Finland.

**Preliminary examiners**
Professor Karsten Voss, Bergische Universitat Wuppertal, Germany;
Dr. Joakim Widén, Uppsala University, Sweden.

**Opponent**
Professor Per Heiselberg, Aalborg University, Denmark

Aalto University publication series
**DOCTORAL DISSERTATIONS** 18/2014



ISBN 978-952-60-5562-6
ISBN 978-952-60-5563-3 (pdf)
ISSN-L 1799-4934
ISSN 1799-4934 (printed)
ISSN 1799-4942 (pdf)
http://urn.fi/URN:ISBN:978-952-60-5563-3

Unigrafia Oy
Helsinki 2014

Finland

Aalto University

# Abstract

Aalto University, P.O. Box 11000, FI-00076 Aalto www.aalto.fi

**Author**
Sunliang Cao

**Name of the doctoral dissertation**
Matching analysis for on-site building energy systems involving energy conversion, storage and hybrid grid connections

**Publisher** School of Engineering

**Unit** Department of Energy Technology

**Series** Aalto University publication series DOCTORAL DISSERTATIONS 18/2014

**Field of research** Energy Engineering

**Manuscript submitted** 1 November 2013 **Date of the defence** 28 March 2014

**Permission to publish granted (date)** 31 January 2014 **Language** English

☐ **Monograph** ☒ **Article dissertation (summary + original articles)**

**Abstract**

Under the background that all new buildings in EU should be nearly zero-energy buildings (nZEB) from the year of 2021, the energy and building industries are progressing towards the direction of decreased local building energy demand and enhanced on-site renewable energy production. This, on one hand, leads to the continuously decreased annual primary energy consumption/equivalent $CO_2$ emission, whereas on the other hand it brings in the matching problem between the on-site generation and local building demand. Considering the fact that the renewable energy fraction in the hybrid grid networks in EU is not likely to reach 100% by the year of 2021, the undesirable mismatch is an inevitable side-effect of low-energy and zero-energy buildings. However, the scientific gap is that there is a lack of comprehensive methodology for the matching analysis of the increasingly complicated on-site hybrid energy systems involving all the energy forms, energy conversions, diversified storage types and hybrid grid connections. Therefore, the objective of this thesis is to set up a methodology to close the aforementioned gap. Correspondingly, six extended matching indices are defined for six aspects of on-site matching situation based on the extension of two basic matching indices. Furthermore, a topology is proposed for a comprehensive understanding and formulation of the extended indices. In order to show the applicability of these extended indices, a thorough matching analysis is conducted for the components of on-site hybrid renewable energy systems in two office buildings with distinct climate conditions. Moreover, in order to overcome the complexity brought in by the six extended matching indices, one evolved index is defined. By the mutual investigation of the evolved index and the extended matching indices, both the overall matching capability and the detailed specific matching aspects can be comprehensively illustrated, which has been proved in an example for a micro-cogeneration application.

With the aid of the methodology developed in this thesis, the matching caused by the diversified treatments of the excess on-site energy production can be quantitatively compared and analysed. For example, the matching capabilities can be compared between the two options for the treatment of excess on-site photovoltaic production: one is to directly export the excess production to the electrical grid, and the other one is to process the electrical-thermal energy conversion for recharging the hot water storage tank. Thereafter, a solution with better matching capability can be achieved. The general outcome shows that the methodology developed in this thesis is a powerful tool in aiding the analysis, design and control of the increasingly complicated on-site energy systems in buildings.

**Keywords** Matching indices; Matching analysis; Mismatch; Building; Renewable feed-in; Hybrid grid networks.

**ISBN (printed)** 978-952-60-5562-6 **ISBN (pdf)** 978-952-60-5563-3

**ISSN-L** 1799-4934 **ISSN (printed)** 1799-4934 **ISSN (pdf)** 1799-4942

**Location of publisher** Helsinki **Location of printing** Helsinki **Year** 2014

**Pages** 138 **urn** http://urn.fi/URN:ISBN:978-952-60-5563-3

# Preface

This doctoral thesis is based on the doctoral study conducted between 2010 – 2014 in Department of Energy Technology, School of Engineering, Aalto University, Finland. The study has been mainly financially supported by the School of Engineering, Aalto University. Moreover, KURKE Project (Finnish: Kunnallisen rakentamisen kestävät energiaratkaisut, toteutustavat ja ohjaus; English: Sustainable energy solutions for municipal buildings), TEKES RYM-SY project, SAGA project, Helsinki University of Technology Foundation, and K.V. Lindholms Stiftelse partially support this doctoral study.

I would like to sincerely acknowledge my supervisor Professor Kai Sirén and my instructor Dr. Ala Hasan. They have both provided me abundant knowledge, advice, experience and encouragement. They have always been very patient for me upon different kinds of questions and difficulties met in my study and research. With their valuable help, my doctoral period is very fruitful, and I enjoyed the moments whenever I met any challenging research questions. I clearly remember that Professor Kai Sirén, Dr. Ala, and I spent several hours in discussing one involved research topic. I enjoyed this kind of debate and discussion, where the new knowledge and inspiration arose. Most important, they taught me the path from a young student towards a researcher. Moreover, I also would like to acknowledge Dr. Juha Jokisalo's instruction during the KURKE project; I have learnt lots of practical research experience upon the standard and low-energy building systems from Dr. Juha, and he has been always very kind for both of my studies and life in Finland.

I also would like to express my acknowledgement for my colleagues' help during my doctoral period. I would like to acknowledge Simo Kilpeläinen, Matti Palonen, Lauri Nissinen, and Petteri Kivivuori for their important help in the laboratory work; acknowledge Lari Eskola for his help in my practical life in Espoo and Helsinki; acknowledge Mohamed Hassan and Ayman Mohamed's help in my doctoral studies; acknowledge Janne Hirvonen's help who was also my classmate during my master's programme. Meanwhile, the secretaries of Mirka Seppälä, Saija Kaljunen and Seija Erander-Luukkanen provided me lots of help in the practical issues, such as conference travelling plans, during my doctoral period.

I would like to especially thank my parents for their great encouragement for my doctoral study and life. They provide me confidence and courage for overcoming any difficulties met in my life.

Doctoral period is not a short time. I myself have experienced many unforgettable things during these several years, both for the study and my personal life. Life is always a journey. There will be sunny days and beautiful views along the journey, and there will also be inevitable rainy days and disappointed views along the journey. Yes, it is sometimes unpredictable and mysterious, but never gives up the confidence and endeavour. With the best wishes in my heart, I am looking forward to the new journey ahead of me.

Sunliang Cao

Espoo, Finland

# Table of contents

## List of original publications

I. Sunliang Cao, Ala Hasan, and Kai Sirén, Analysis and solution for renewable energy load matching for a single-family house, Energy and Buildings, 65 (2013) 398-411. [Online]. Available: http://www.sciencedirect.com/science/article/pii/S0378778813003514.

II. Sunliang Cao, Ala Hasan, and Kai Sirén, On-site energy matching indices for buildings with energy conversion, storage and hybrid grid connections, Energy and Buildings, 64 (2013) 423-438. [Online]. Available: http://www.sciencedirect.com/science/article/pii/S0378778813003150.

III. Sunliang Cao, Ala Hasan, and Kai Sirén, Matching analysis for on-site hybrid renewable energy systems of office buildings with extended indices, Applied Energy 113 (2014) 230-247. [Online]. Available: http://www.sciencedirect.com/science/article/pii/S0306261913005977.

IV. Sunliang Cao, Ayman Mohamed, Ala Hasan, and Kai Sirén, Energy matching analysis of on-site micro-cogeneration for a single-family house with thermal and electrical tracking strategies, Energy and Buildings 68 (2014), pp. 351-363. [Online]. Available: http://www.sciencedirect.com/science/article/pii/S0378778813006191.

## Author's contribution

Sunliang Cao is the principle author in all the four original publications (I, II, III, and IV). The proposal of the concept, numerical simulation, analysis of the data, and writing of the papers, are all conducted by Sunliang Cao in these four journal papers. The co-authors of Dr. Ala Hasan and Professor Kai Sirén provided the supervision for the research work of all the four publications. In original publication IV, the second author Ayman Mohamed helped in making the micro-cogeneration models and provided partial support for the analysis of the comparison between matching and net primary energy consumption with bio-fuel.

## Nomenclature and Abbreviation

ACH: Air changes per hour

AHU: Air handling unit

$C_{eoff\text{-}c}$: Cooling power generated by the electrically driven cooling machines by the off-site part of the electricity (kW)

$C_{eon\text{-}c}$: Cooling power generated by the electrically driven cooling machines by the on-site part of the electricity (kW)

$C_{eoff\text{-}h}$: Simultaneous cooling powers generated by the evaporators of the electrically driven heating machines by the off-site part of the driving electricity (kW)

$C_{eon\text{-}h}$: Simultaneous cooling powers generated by the evaporators of the electrically driven heating machines by the on-site part of the driving electricity (kW)

$C_{hoff\text{-}c}$: Cooling power generated by the thermally driven cooling machines by the off-site part of the heat (kW)

$C_{hon\text{-}c}$: Cooling power generated by the thermally driven cooling machines by the on-site part of the heat (kW)

CHP: Combined heat and power

COP: Coefficient of performance

$CS_{off}$: Net off-site part of the cooling power sent to cold storage, charge in '+' sign, and discharge in '-' sign (kW)

$CS_{on}$: Net on-site part of the cooling power sent to cold storage, charge in '+' sign, and discharge in '-' sign (kW)

DHW: Domestic hot water

dt: The time-step used in the research

$E_{off\text{-}h}$: Off-site part of the electrical power sent to the electrically driven heating machines (kW)

$E_{on\text{-}h}$: On-site part of the electrical power sent to the electrically driven heating machines (kW)

$E_{off\text{-}c}$: Off-site part of the electrical power sent to the electrically driven cooling machines (kW)

$E_{on\text{-}c}$: On-site part of the electrical power sent to the electrically driven cooling machines (kW)

$ES_{off}$: Net off-site part of the electrical power sent to electrical storage, charge in '+' sign, and discharge in '-' sign (kW)

$ES_{on}$: Net on-site part of the electrical power sent to electrical storage, charge in '+' sign, and discharge in '-' sign (kW)

ETTR: Electrical to thermal ratio

EU: European Union

$F_{eg}$: Interactive electrical power with the electrical grid, exporting in '+' sign, and importing in '-' sign (kW)

$F_{dh}$: Interactive heating power with the heating grid, exporting in '+' sign, and importing in '-' sign (kW)

$F_{dc}$: Interactive cooling power with the cooling grid, exporting in '+' sign, and importing in '-' sign (kW)

FSOC: Fractional state of charge

G: On-site generated power (kW)

GSHP: Ground source heat pump

$G_{elec}$: Electrical power generated by the on-site electrical energy production system (kW)

$G_{h\_th}$: Heating power generated by the on-site thermal energy production system (kW)

$G_{c\_th}$: Cooling power generated by the on-site thermal energy production system (kW)

$H_{eoff\text{-}c}$: Simultaneous heating power generated by the condenser of the electrically driven cooling machines by the off-site part of the driving electricity (kW)

$H_{eon\text{-}c}$: Simultaneous heating power generated by the condenser of the electrically driven cooling machines by the on-site part of the driving electricity (kW)

$H_{eoff\text{-}h}$: Heating power generated by the electrically driven heating machines by the off-site part of the electricity (kW)

$H_{eon\text{-}h}$: Heating power generated by the electrically driven heating machines by the on-site part of the electricity (kW)

$H_{hoff\text{-}c}$: Simultaneous heating power generated by the condensers of the thermally driven cooling machines by the off-site part of the heat (kW)

$H_{hon\text{-}c}$: Simultaneous heating power generated by the condensers of the thermally driven cooling machines by the on-site part of the heat (kW)

$H_{off\text{-}c}$: Off-site part of the heating power sent to the thermally driven cooling machines (kW)

$H_{on\text{-}c}$: On-site part of the heating power sent to the thermally driven cooling machines (kW)

$HS_{off}$: Net off-site part of the heating power sent to heat storage, charge in '+' sign, and discharge in '-' sign (kW)

$HS_{on}$: Net on-site part of the heating power sent to heat storage, charge in '+' sign, and discharge in '-' sign (kW)

HTF: Heat transfer fluid

HWST: Hot water storage tank

HX: Heat exchanger

L: Load power (kW)

$L_{elec}$: Electrical load power excluding the electrical load from the electrically driven heating and cooling machines (kW)

$L_{heat}$: Heating load power excluding the heating load from the thermally driven cooling machines (kW)

$L_{cold}$: Cooling load power (kW)

ICE: Internal combustion engine

$l_e$: Loss of on-site electrical power during the distribution process (kW)

$l_h$: Loss of on-site heating power during the distribution process (kW)

$l_c$: Loss of on-site cooling power during the distribution process (kW)

mCHP: micro combined heat and power

MPP: Maximum power point

nZEB: Nearly zero-energy buildings

OEF: On-site energy fraction

OEM: On-site energy matching

OEFe: On-site electrical energy fraction

OEFh: On-site heating energy fraction

OEFc: On-site cooling energy fraction

OEMe: On-site electrical energy matching

OEMh: On-site heating energy matching

OEMc: On-site cooling energy matching

ORC: Organic Rankin Cycle

PV: Photovoltaic

$P_{amb}$: Heating power entering the thermal process of the conversion machine (electrically driven heating machine, electrically driven cooling machine, or thermally driven cooling machine) from the ambient outside the boundary of the building (kW)

$P_{drive,on}$: On-site part of the heating power entering the thermal process of the machine, which is directly converted from the on-site part of the power driving the machine (kW)

$P_{drive,off}$: Off-site part of the heating power entering the thermal process of the machine, which is directly converted from the off-site part of the power driving the machine (kW)

r: On-site proportion of the heating or cooling power generated by the electrically driven heating machine, the electrically driven cooling machine, or the thermally driven cooling machine

REe: Renewable electrical

RER: Renewable energy ratio

REth: Renewable thermal

$t_1$: Starting point of the time span

$t_2$: Ending point of the time span

# 1 Introduction

With global warming as one of the most serious concerns throughout the world, significant research efforts have been

continuously focusing on the solutions to reduce primary energy consumption and equivalent $CO_2$ emission. Two main tracks are normally followed: one is to reduce the on-site energy demands by various solutions, such as implementation of high-performance building envelopes [1,2,3,4] and improvement of the efficiency of heating/cooling delivery and recovery systems [5,6,7]; the other one is to establish on-site renewable energy systems [8,9,10] together with diversified storage components [2,11,12,13]. These two tracks focus on on-site demand and production aspects, respectively, and both lead to reduction of primary energy consumption and equivalent $CO_2$ emission. Due to the intensive research efforts focusing on these aspects, the building system is progressing towards lower primary energy consumption and lesser environmental impact. As a result, the objective of low-energy/emission or net zero-energy/emission buildings will be realised in the near future. In the European Union (EU), a legislation by the European Parliament regulates that all new buildings built from 2021 onwards should be nearly zero-energy buildings (nZEB) [14,15,16]. Although other regions in the world might not have such strict legislations, it is a noteworthy hint about the future trend in the global building industry.

However, this trend brings in a new challenge, which should be carefully handled — the so-called matching problem. Taking an all-electric nZEB with on-site PV generation as an example, a significant amount of energy should be exported to the grid in the summer time to balance the energy imported in the winter time, as shown in Figure 1. A similar problem occurs to other on-site energy systems, such as wind turbine, for reaching the low or even zero primary energy consumption / equivalent $CO_2$ emission, but it is at a different time or seasonal scale compared to PV. The resulting situation is that a building might have a severe mismatch characteristic, even though it reaches the annual net zero-energy/emission balance. This problem is a potential security issue for the electrical grid, as large amounts of distributed electrical generation with a severe mismatch characteristic significantly increase the probability to destabilise the voltage limitations of the grid [17,18,19]. More specifically, the main technical challenge is that the distribution grid is traditionally designed for handling the peak load instead of the peak on-site generation. When the on-site generation peak is higher than the load peak, which can be particularly happened in high latitude countries for reaching the annual net zero energy balance, the voltage limitation in the grid and grid components have the risk to be exceeded or overloaded [20,21]. Although these technical problems might be solved by replacing and upgrading the grid cables, optimizing the grid topologies, resizing the generators or rearranging the voltage regulations in the substations [20,21], the enhancement of on-site matching capability is a much more cost-effective way to avoid the high cost for renovating the electrical grid infrastructures. Moreover, an important drive for the matching analysis is due to the imbalance between the import and export grid tariffs. The most common situation is that the export tariff is lower than the import tariff (including the situation that there is no export tariff), such as in most EU countries [22]. Furthermore, in some

countries such as in Germany and Italy, there has been a policy to remunerate the self-consumed PV electricity with a premium tariff [23]. This means that, from an economic point of view, the high on-site matching capability will also be a benefit for the economical feasibility of the on-site energy systems. These all make the matching analysis meaningful and indispensable for low-energy and net zero-energy buildings.

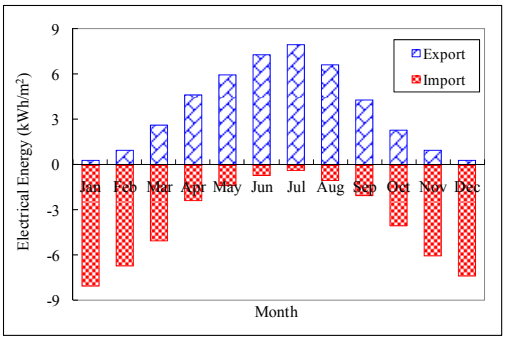

Figure 1. The monthly mismatch for an all-electric nZEB with on-site PV [Original publication III].

There has been a lot of research on the analysis of electrical matching problem for on-site electrical generation systems, such as PV and wind turbine, due to their straightforward handling process [24,25,26,27,28,29]. However, with the fast progress of the energy and building technologies, the traditional methodologies for the electrical matching analysis are less likely to meet the requirements. Firstly, the on-site energy systems often involve two or all of the electrical, heating, and cooling energy forms, especially in hybrid energy systems, such as photovoltaic-thermal collectors for electrical and heating energy forms. Secondly, the on-site energy systems often involve energy conversion processes between different energy forms, as, for example, in the case of a PV-assisted ground source heat pump (GSHP) converting electrical energy to heating or cooling energy. Thirdly, the on-site energy systems are usually equipped with various energy storage systems, such as battery for the electrical storage of PV system and hot water storage tank for the thermal storage of solar thermal collectors. Fourthly, the on-site energy systems are more and more commonly bi-directionally connected to various types of grid networks. These bi-directional connections allow the annual primary energy/equivalent emission balance be more easily managed by treating the grid networks as a virtual energy storage. The electrical grid with a distributed feed-in option is currently commonly available in many countries, including Belgium [30], the UK [31], and Germany [32,33]. Moreover, in many EU countries, heating generated by distributed on-site solar thermal collectors has been successfully fed into district heating systems, and the technology has been experiencing fast development [34]. Nevertheless, except in several highly developed cities, such as Barcelona [35] and Helsinki [36], the technology of district cooling itself is not widely used. This leads to the fact that the distributed feed-in option for the district cooling has not been practically realized, because the first step is to wait for the maturity of the district cooling technology itself.

However, the distributed feed-in technologies used in the thermal heating grids have a great potential to apply to the thermal cooling grid. And the author of this thesis believes that the hybrid grid networks of electrical, heating, and cooling with distributed feed-in options will be realized in the near future, while nZEBs will be the nodes inside the hybrid networks. Hereby, the matching problem mentioned for the electrical aspect will also be extended to the heating and cooling aspects, especially when the on-site heating/cooling generation unit is dependant on the intermittent renewable energy resources, such as solar thermal energy. For example, if the heating grid (district heating network) is designed according to the peak heating load, the high penetration of on-site solar thermal heating will be a potential risk for the stability of the heating transmission networks and relating components. Thus, the high matching capability between the on-site generation and demand will still be an important solution to avoid or reduce the cost for renovating the heating and cooling grids so that it can be compatible with more on-site distributed generation units in the future. Currently there is no detailed reference upon the import and export tariffs for heating/cooling grids. However, no matter what is the relation between the import and export tariffs of the heating/cooling grids, the matching capability will still be an important factor for influencing the economical feasibility of the on-site thermal energy generation systems.

The abovementioned points give rise to suitable criteria that should be set up to quantitatively assess the matching capability of on-site energy systems, involving all energy forms, energy conversions, diversified energy storage solutions, and hybrid electrical and thermal grid connections. Moreover, due to various energy conversions, storage systems and hybrid grid connections, the treatment of excess on-site energy production is also becoming diversified, adding complexity to the matching analysis of hybrid on-site energy systems. However, the scientific gap is that there is a lack of comprehensive methodology for the matching analysis of the increasingly complicated on-site hybrid energy systems with the aforementioned challenges and complexities. Therefore, the objective of this thesis is to set up a methodology to close this scientific gap, and it is aimed that this methodology can be helpful for aiding the analysis and design of low-energy and zero-energy buildings. Moreover, it should be mentioned that this thesis is mainly focused on the energy analysis aspect, whereas the economical analysis is not the main theme. In the following sections, the review of the traditional basic indices and the proposal of the extended indices are presented in Section 2. Thereafter, in Section 3, the extended indices are implemented for the design and analysis of the on-site energy components in two advanced office buildings with enhanced hybrid on-site renewable energy systems and bi-directionally connected hybrid grid connections. In Section 4, the evolvement of the extended indices is conducted to overcome the shortages of the extended indices. There is a summary of the new contributions in Section 5, and Section 6 provides the conclusion. In the end, Section 7 lists the future works relating to this thesis.

# 2 Assessment criteria

## 2.1 Traditional basic indices (Original publications I and II)

Since the 1970s, a simple concept of "solar heating fraction" has started to be used for evaluating the proportion of the heating demand covered by on-site solar heating production [37, 38]. Since then, various indices have emerged to assess the matching between the demand and generation for on-site thermal or electrical energy systems, as listed in Table 1. Although the notations are various (Table 1), there are essentially two basic matching indices. In this thesis, these two basic matching indices are termed on-site energy fraction (OEF) and on-site energy matching (OEM). OEF indicates the proportion of the load covered by the on-site generation, while OEM indicates the proportion of the on-site generation consumed in the building and system rather than being exported or dumped. The equations of the two basic indices are presented as follows:

$$\mathrm{OEF} = \frac{\int_{t_1}^{t_2} \mathrm{Min}[G(t);\, L(t)]dt}{\int_{t_1}^{t_2} L(t)dt}\ ; \quad 0 \le \mathrm{OEF} \le 1 \qquad (1)$$

$$\mathrm{OEM} = \frac{\int_{t_1}^{t_2} \mathrm{Min}[G(t);\, L(t)]dt}{\int_{t_1}^{t_2} G(t)dt}\ ; \quad 0 \le \mathrm{OEM} \le 1 \qquad (2)$$

where G(t) and L(t) are the on-site generated power and load power, respectively, at an instantaneous time, t. 'dt' is the differential time difference, which is in the simulation handled as the computational time-step, e.g. 1 minute. The variables '$t_1$' and '$t_2$' represent the starting and ending points of the time span, respectively. By adjusting $t_1$, $t_2$ and dt, the indices of a certain period can be calculated, for instance daily, monthly or yearly instances. The main principles of OEF and OEM are additionally depicted in Figure 2. As shown in Figure 2, OEF is equal to the ratio of the area of section III to the total area of sections I and III, while OEM is equal to the ratio of the area of section III to the total area of sections II and III. Better matching is represented by higher values of OEF and OEM, simultaneously. The best scenario for the matching capability is when OEF and OEM are both equal to unity, which indicates that the load is entirely covered by the on-site generation and the on-site generation is entirely consumed in the building and system. It should be additionally mentioned that a coarser time-step 'dt' would possibly lead to an overestimation of the matching capability. For example, Figure 3 presents a simple example of the electrical demand profiles with 1 minute (min) and 1 hour (hr) resolutions for a time span of six hours, while a hypothetical constant generation is at 2 kW. With 1 min resolution, several peak spikes of the electrical demand curve are above the generation level, whereas with 1 hr resolution the electrical demand curve is completely below the generation level as the spikes are averaged to a smoother profile. As a result, by using the 1 hr resolution, both the OEF (1.00) and OEM (0.56) are overestimated compared to the results (0.71

and 0.40, respectively) by using 1 min resolution. Although finer resolution leads to a more accurate matching result, the computational effort will be much heavier. Moreover, most of the public available database is also based on 1 hr resolution, such as the weather files, which all lead to the fact that the prevailing resolutions in the building simulation is still with 1 hr. This thesis is focused on the development of the methodology for the analysis of the matching capability, whereas the specific impact of the resolution on the matching capability is not the focused theme in this thesis, but it will be investigated in the future work as presented in Section 7. Generally speaking, during a simulation or analysis with certain time-step 'dt', it should always be assumed that an energy storage or buffer is existing in the system whose capacity can level off the fluctuations of the mismatch between the demand and generation within the time-step 'dt'.

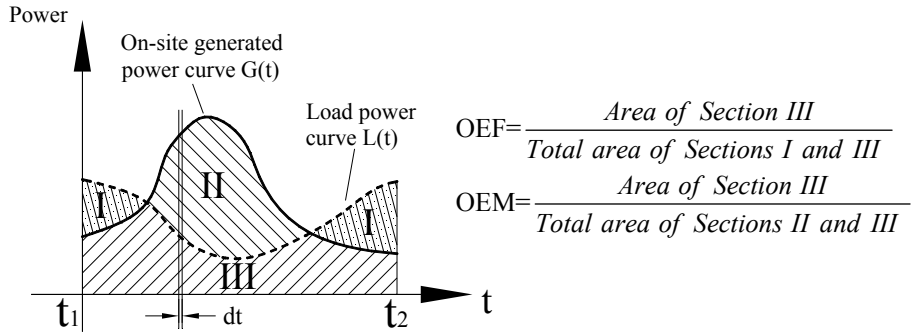


Figure 2. The main principle for the two basic indices [Original publication II].

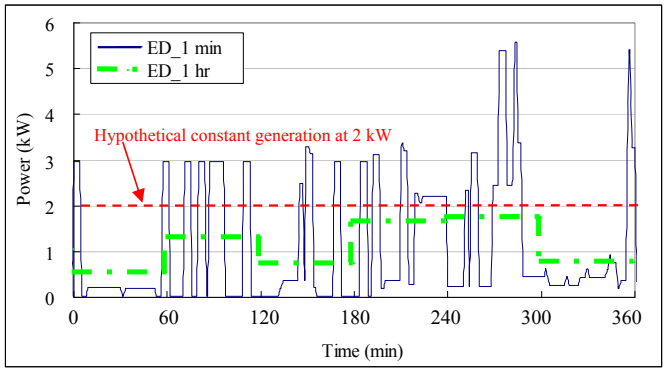


When dt = 1 min,
OEF = 0.71
OEM = 0.40

When dt = 1 hr,
OEF = 1.00
OEM = 0.56

Figure 3. The averaging effect on the matching capability by the resolutions of 1 min and 1 hr. The red horizontal dash line is the hypothetical constant generation level at 2 kW. (ED: Electrical Demand).

Table 1. Various reviewed matching indices refer to OEF and OEM.

| OEF | OEM |
|---|---|
| solar heating fraction [37,38]; | excess supply percentage index [24]; |
| solar fraction [26, 39]; | renewable energy matching [Original publication I]. |
| load match index [27] ; | |
| cover factor [29]; | |
| self-consumption factor [40]; | |
| self-sustenance index [25]; | |
| shared area percentage index [24]; | |
| renewable energy fraction [Original publication I]. | |

Among the reviewed indices listed in Table 1, the "renewable energy faction" and the "renewable energy matching" are developed by the author of this thesis, as presented in Equation (3) and Equation (4):

$$REF=\frac{\int_{t_1}^{t_2} Min[(G(t)-ES(t)-HS(t)), L(t)]dt}{\int_{t_1}^{t_2} L(t)dt} \quad (3)$$

$$REM=\frac{\int_{t_1}^{t_2} Min[G(t), (L(t)+ES(t)+HS(t))]dt}{\int_{t_1}^{t_2} G(t)dt} \quad (4)$$

ES(t) is the net on-site generated electrical power sent to the battery (charging status with positive value; discharging status with negative value). HS(t) is the on-site generated electrical power sent to recharge the DHW storage tank. By using these two equations, the effects of the electrical battery and the recharging of the DHW storage tank can be taken into account. However, REF and REM are still only focused on the electrical aspect, which significantly limits their usages.

Furthermore, as mentioned in Section 1, with the fast development of energy technology, the matching analysis should take into account the factors of all energy forms, energy conversions, diversified storage systems, and hybrid bi-directionally connected hybrid grid networks. However, the basic matching indices, as presented in Equations (1) and (2), are not able to handle all these factors. Thus, new matching indices should be defined to cope with the challenges.

## 2.2 Generalised extended indices with one topology (Original publication II)

### 2.2.1 The topology for generalised matching analysis

In order to cope with the aforementioned challenges, six matching indices are defined based on the extension of two basic matching indices. Three of these are based on the extension of OEF: on-site electrical energy fraction (OEFe), on-site heating energy fraction (OEFh), and on-site cooling energy fraction (OEFc); the other three are based on the extension of OEM: on-site electrical energy matching (OEMe), on-site heating energy matching (OEMh), and on-site cooling energy matching (OEMc); the postfixes e, h, and c represent the electrical, heating, and cooling energy,

respectively. **It should be emphasised that the "off-site" energy mentioned in this thesis is the energy imported or converted from the grid; whereas, the "on-site" energy means the energy generated or converted from the on-site energy systems excluding the portion imported or converted from the grid.** Therefore, the concept of "on-site" is not simply judged by the location where the energy is generated, but is judged by the origin of the energy with respect to the grids. For example, the heating energy generated by an electrical heater located in a house can contain both the on-site and off-site heating portions, under the situation that the off-site heating portion is converted from the electrical energy that is imported from the electrical grid, while the on-site heating portion is converted from the electrical energy that is generated by an on-site micro-wind turbine. Furthermore, there is a special treatment for the concept of on-site and off-site cooling power generated by the energy conversion machines (electrically or thermally driven cooling machines), which will be described latter.

The understanding of the definition of the "on-site" and "off-site" energy is the essential fundamental for the formulation of the extended indices. It is particularly important to re-emphasize that the "on-site" and "off-site" are not simply judged by the location where the energy is generated. If the "on-site" energy was only treated according to the location where the energy is generated, it would neglect the impact of the conversion processes. For example, it would lead to the fact that, even if all the electrical energy were imported from the electrical grid, all the heating energy generated by an electrical heater was fully on-site. This would mislead the on-site matching results for the heating aspect, especially when the heating demand is for instance met by both the aforementioned electrical heater and a solar thermal collector. The detailed handling process of the energy conversion processes will be described in detail in the latter Section 2.2.2.

Six extended indices are developed based on a topology defined by the author of this thesis. Before the presentation of the extended indices' equations, this topology should be firstly introduced. As shown in Figure 4, the topology is composed of three sub-parts: electrical sub-part, heating sub-part, and cooling sub-part, each of which is centred by a distribution centre. Each distribution centre connects to a generation box, a storage box, a grid box, and a load box. The generation box contains certain on-site generation unit which directly generates the on-site energy without going through the electrical-thermal or thermal-electrical conversion processes, such as an on-site PV producing on-site electrical power $G_{elec}(t)$ in the box of the electrical generation unit, a solar thermal collector producing on-site heating power $G_{h\_th}(t)$ in the box of the heating generation unit, and a ground water free cooling system producing on-site cooling power $G_{c\_th}(t)$ in the box of the cooling generation unit. The electrical consumption of possible hydronic circulating devices during the on-site cooling generation process $G_{c\_th}(t)$ and the on-site heating generation process $G_{h\_th}(t)$ are considered to be part of the electrical load, for example the pump power consumption for free groundwater cooling or

the fan power consumption for the solar thermal air heater.

The storage box contains a certain type of energy storage system, such as an electrical battery in the box of electrical storage, a hot water storage tank in the box of heat storage, and a cold water storage tank in the box of cold storage. There are two arrow lines between each distribution centre and the corresponding storage box. These two arrow lines represent the net on-site and off-site part of the power sent to the storage: charge in the '+' sign, and discharge in the '-' sign. Furthermore, between each distribution centre and the grid box, there is one arrow line representing the energy interactions between the building system and a certain type of the grid: exporting in the '+' sign, and importing in the '-' sign. The load box contains a certain type of load, excluding the load from the conversion box.

To carry out the energy conversion processes, each two of the three sub-parts are interfaced by a conversion box. These are the box of "electrically driven heating machines" on the interface of the electrical and heating sub-parts, the box of "electrically driven cooling machines" on the interface of the electrical and cooling sub-parts, and the box of "thermally driven heating machines" on the interface of the heating and cooling sub-parts. The "electrically driven heating machines" may include e.g. a direct electrical heater, an electrically driven ground source heat pump, and other devices. The "electrically driven cooling machines" may include e.g. an electrically driven vapour compression chiller and others. The "thermally driven heating machines" may include e.g. a thermally driven absorption chiller, a thermally driven adsorption chiller, and others. Each conversion box connects with four arrow lines. Taking the "electrically driven heating machines" as an example, two arrow lines represent the on-site and off-site electrical driving powers $E_{on\text{-}h}(t)$ and $E_{off\text{-}h}(t)$, respectively, while the other two arrow lines represent the heating powers $H_{eon\text{-}h}(t)$ and $H_{eoff\text{-}h}(t)$ generated by the electrically driven heating machines by the on-site and off-site parts of the electricity, respectively. From the standpoint of an electrical sub-part, $E_{on\text{-}h}(t)$ and $E_{off\text{-}h}(t)$ are also electrical loads: this is the reason why the electrical load box should exclude the electrical load from the electrically driven heating machines. Other conversion boxes follow a manner similar to that described for the "electrically driven heating machines".

The long blue dash-dot rectangle in Figure 4 represents the boundary of the building. Thus, the grid boxes are beyond the building boundary. Furthermore, it should be mentioned that the cooling energy is a virtual concept, because the cooling energy essentially means the heating energy removed from certain space. However, the cooling energy concept is retained for the reason of consistency with the analysis of electrical and heating energy forms and for the reason of convenience of the analysis under the existence of the cooling grid. To show the virtual concept, all the arrow lines in Figure 4 representing cooling powers are dashed lines.

The colours of the arrow lines shown in Figure 4 are meant to better illustrate the topology for those with access to a colour printer. The purple arrow lines represent the loads which can be "seen" by a certain distribution centre. The orange arrow lines represent the interactive power exchanges between the distribution centre and a certain grid. The rest of the arrow lines have two colours, green and black, representing the on-site and off-site power, respectively.

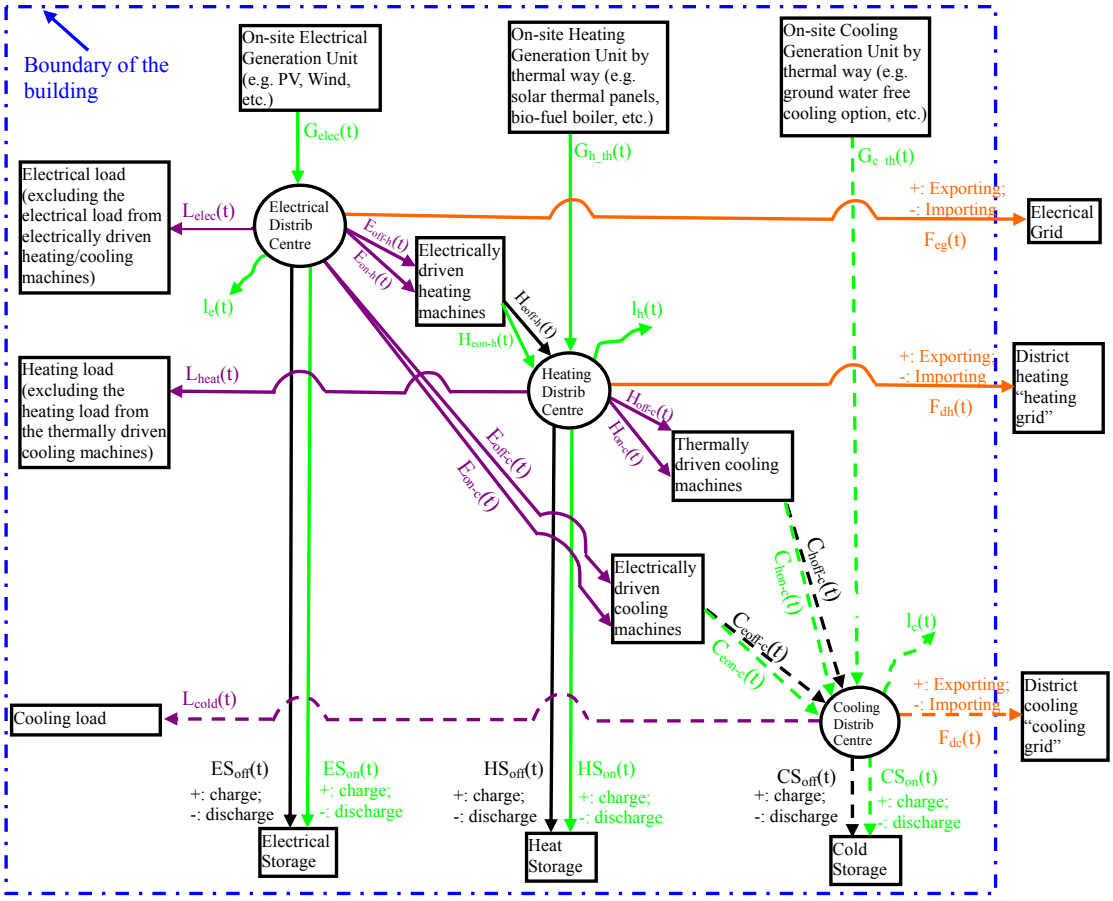


Figure 4. The topology of the extended matching indices for electricity, heating, and cooling [Original publication II].

### 2.2.2 Equations of extended indices and special treatments

Based on the topology shown in Figure 4, the six extended indices are formulated in Equations (5)-(10).

The extended indices for on-site energy fraction (OEF) are as follows:

$$OEFe = \frac{\int_{t_1}^{t_2} Min[G_{elec}(t) - ES_{on}(t) - l_e(t);\ L_{elec}(t)+E_{off\text{-}h}(t)+E_{on\text{-}h}(t)+E_{off\text{-}c}(t)+E_{on\text{-}c}(t)]dt}{\int_{t_1}^{t_2} [L_{elec}(t)+E_{off\text{-}h}(t)+E_{on\text{-}h}(t)+E_{off\text{-}c}(t)+E_{on\text{-}c}(t)]dt} \quad (5)$$

$$OEFh = \frac{\int_{t_1}^{t_2} Min[G_{h\_th}(t) + H_{eon\text{-}h}(t) - HS_{on}(t) - l_h(t);\ L_{heat}(t)+H_{off\text{-}c}(t)+H_{on\text{-}c}(t)]dt}{\int_{t_1}^{t_2} [L_{heat}(t)+H_{off\text{-}c}(t)+H_{on\text{-}c}(t)]dt} \quad (6)$$

$$OEFc = \frac{\int_{t_1}^{t_2} Min[G_{c\_th}(t)+C_{hon\text{-}c}(t) + C_{eon\text{-}c}(t) - CS_{on}(t) - l_c(t);\ L_{cold}(t)]dt}{\int_{t_1}^{t_2} L_{cold}(t)dt} \quad (7)$$

The extended indices for on-site energy matching (OEM) are as follows:

$$OEMe = \frac{\int_{t_1}^{t_2} Min[G_{elec}(t);\ L_{elec}(t)+E_{on\text{-}h}(t)+E_{on\text{-}c}(t)+ES_{on}(t)+l_e(t)]dt}{\int_{t_1}^{t_2} G_{elec}(t)dt} \quad (8)$$

$$OEMh = \frac{\int_{t_1}^{t_2} Min[G_{h\_th}(t)+H_{eon\text{-}h}(t);\ L_{heat}(t)+H_{on\text{-}c}(t)+HS_{on}(t)+l_h(t)]dt}{\int_{t_1}^{t_2} [G_{h\_th}(t)+H_{eon\text{-}h}(t)]dt} \quad (9)$$

$$OEMc = \frac{\int_{t_1}^{t_2} Min[G_{c\_th}(t)+C_{hon\text{-}c}(t)+C_{eon\text{-}c}(t);\ L_{cold}(t)+CS_{on}(t)+l_c(t)]dt}{\int_{t_1}^{t_2} [G_{c\_th}(t)+C_{hon\text{-}c}(t)+C_{eon\text{-}c}(t)]dt} \quad (10)$$

The nomenclatures of the terms in the equations can be checked in the Nomenclature and Abbreviation section of this thesis. It should additionally be mentioned that in cases in which both the denominator and the numerator are zero in Equations (5)-(10), the index value is one. This means that when there is no load, the on-site energy fraction (OEF) is 100%; likewise, when there is no on-site generation, the on-site energy matching (OEM) is 100%. With respect to the topology of Figure 4, OEFe and OEMe are formulated based on the arrow lines (terms) around the "Electrical distribution centre"; OEFh and OEMh are formulated based on the arrow lines (terms) around the "Heating distribution centre"; OEFc and OEMc are formulated based on the arrow lines (terms) around the "Cooling distribution centre". Take the "Heating distribution centre" as an example. In Equation (6) for OEFh, the terms of "$L_{heat}(t)+H_{on\text{-}c}(t)+H_{off\text{-}c}(t)$" are the heating load, which can be "seen" by the "Heating distribution centre" at the current time-step dt, while the terms of "$G_{h\_th}(t)+H_{eon\text{-}h}(t)-HS_{on}(t)-l_h(t)$" are the available on-site heating power, at the current time-step dt, which can be used for meeting the heating load by taking the direct on-site generation (via on-site heating generation unit by the thermal way), indirect on-site generation (via energy conversion), storage, and loss into account. Thus, the lower one from the comparison of "$L_{heat}(t)+H_{on\text{-}c}(t)+H_{off\text{-}c}(t)$" and "$G_{h\_th}(t)+H_{eon\text{-}h}(t)-HS_{on}(t)-l_h(t)$" is the on-site portion of the heating load which is covered by the on-site heating power at the current time-step dt. In Equation (9) for OEMh, the terms of "$G_{h\_th}(t)+H_{eon\text{-}h}(t)$" are the generated on-site heating power, at the current time-step dt, which can be "seen" by the "Heating distribution centre", while the terms of "$L_{heat}(t)+H_{on\text{-}c}(t)+HS_{on}(t)+l_h(t)$" are the places where the on-site

generated heating power can be consumed at the current time-step. Thus, the lower one from the comparison of "$G_{h\_th}(t)+H_{eon\text{-}h}(t)$" and "$L_{heat}(t)+H_{on\text{-}c}(t)+HS_{on}(t)+l_h(t)$" is the portion of the on-site generated heating power consumed in the building and system at the current time-step dt.

One important point that should be described in detail is the treatment of energy conversion processes in the conversion boxes, namely, in "Electrically driven heating machines", "Electrically driven cooling machines", and "Thermally driven cooling machines". In practice, it is easy to get the overall heating or cooling power generated by these machines, for example the overall generated heating power "$H_{eon\text{-}h}(t)+H_{eoff\text{-}h}(t)$" of an electrically driven heat pump in heating mode is calculated by multiplying the overall electrical driving power "$E_{on\text{-}h}(t)+E_{off\text{-}h}(t)$" by the coefficient of performance (COP) of the heat pump. However, it is not so straightforward to get the on-site ("$H_{eon\text{-}h}(t)$") and off-site ("$H_{eoff\text{-}h}(t)$") heating powers separately. The reason can be explained with the aid of the energy balance depicted in Figure 5 for an electrically driven ground source heat pump (GSHP) in heating mode. According to the energy balance, the overall heating power generated by the GSHP ("$H_{eon\text{-}h}(t)+H_{eoff\text{-}h}(t)$") is equal to the heating power transferred from the ground to the evaporator ("$Q_{ground}$") plus the overall electrical driving power entering the compressor ("$E_{on\text{-}h}(t)+E_{off\text{-}h}(t)$"). Here, $Q_{ground}(t)$ is neither imported nor converted from the grid, so that it is not off-site heating power, but is counted as on-site. Therefore, $H_{eon\text{-}h}(t)$ is equal to the sum of $Q_{ground}(t)$ and $E_{on\text{-}h}(t)$, whereas $H_{eoff\text{-}h}(t)$ is equal to $E_{off\text{-}h}(t)$.

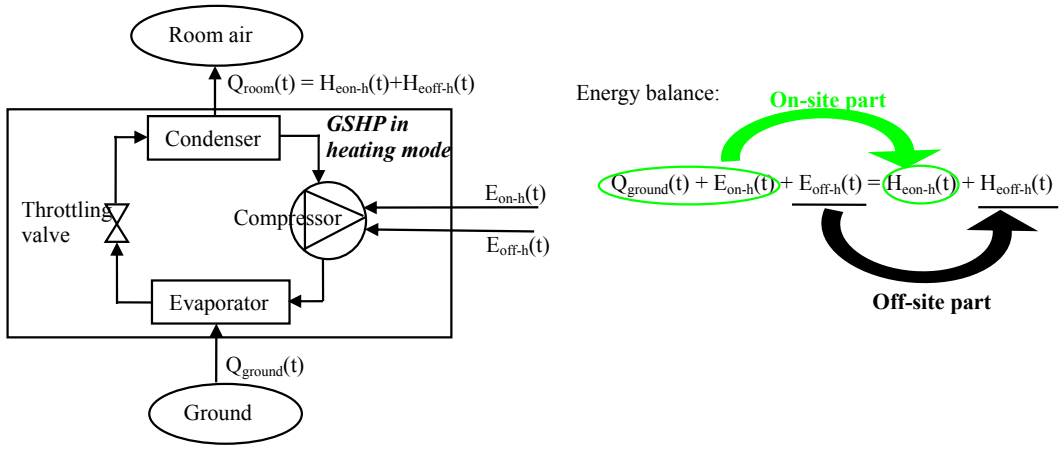


Figure 5. The energy balance of the ground source heat pump in the heating mode [Original publication II].

However, when the GSHP works in the cooling mode, the situation becomes very special. As shown in Figure 6 for the energy balance of GSHP in cooling mode, the heating power absorbed from the room air (the absolute value of "$C_{eon\text{-}c}(t)+C_{eoff\text{-}c}(t)$") plus the overall electrical driving power entering the compressor ("$E_{on\text{-}c}(t)+E_{off\text{-}c}(t)$") are equal to the

heating power transferred from the condenser to the ground ("$Q_{ground}$"). As mentioned in Section 2.2, cooling power is a virtual concept, because it is essentially the heating power removed from a certain space. Thus, although there is no negative value for $C_{eon\text{-}c}(t)$ or $C_{eoff\text{-}c}(t)$, the absolute marks '||' are still illustrated to emphasize the virtual concept. From this balance shown in Figure 6, the separation method for the on-site and off-site parts in the heating mode is no longer effective for the cooling mode. If the same rule as in the heating mode was applied, the entire cooling power generated by GSHP becomes on-site, because it is neither imported nor converted from the grid. However, this treatment actually leads to a situation that any cooling power generated by the conversion machine (electrically or thermally driven cooling machine) is entirely on-site cooling power. In order to solve this problem, a special rule is defined here: in the conversion machine for generating cooling power (electrically or thermally driven cooling machine), the ratio between the on-site and off-site cooling power is equal to the ratio between the on-site and off-site power driving the conversion machine. This is a special rule, because there is a compromise in the physical meaning for this treatment, but it correlates the cooling power with the driving power for the conversion machine.

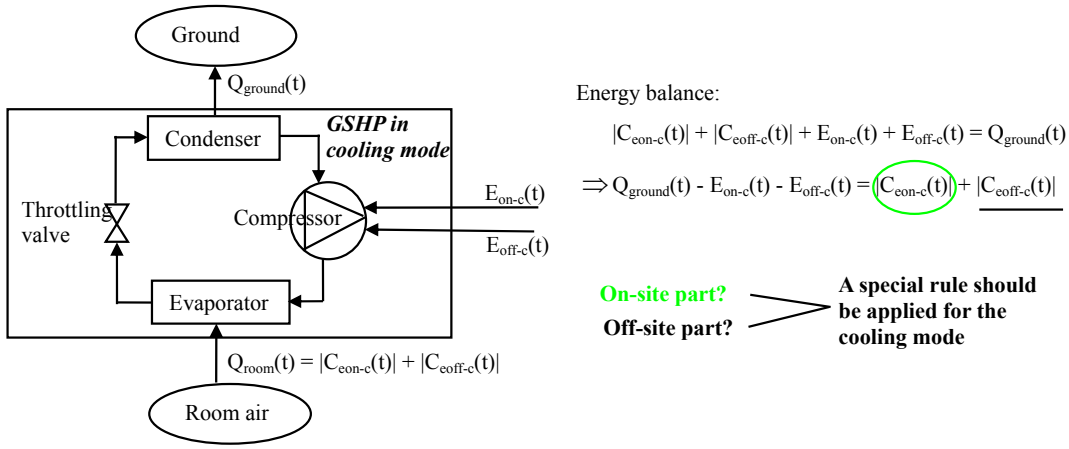


Figure 6. The energy balance of the ground source heat pump in the cooling mode [Original publication II].

In order to generalize the calculation method for the separation of on-site and off-site power generated through the conversion machines, a ratio r is defined to represent the on-site proportion of the generated heating or cooling power from the conversion machine, as presented in Equation (11):

$$r=\frac{H_{eon\text{-}h}(t)}{H_{eoff\text{-}h}(t)+H_{eon\text{-}h}(t)} \text{ or } \frac{C_{eon\text{-}c}(t)}{C_{eoff\text{-}c}(t)+C_{eon\text{-}c}(t)} \text{ or } \frac{C_{hon\text{-}c}(t)}{C_{hoff\text{-}c}(t)+C_{hon\text{-}c}(t)} \quad , \tag{11}$$

while the general calculation method for this ratio r is presented in Equation (12):

$$r=\frac{P_{amb}(t)+P_{drive,on}(t)}{P_{amb}(t)+P_{drive,on}(t)+P_{drive,off}(t)} \tag{12}$$

$P_{drive,on}(t)$ is the on-site part of the heating power entering the thermal process of the machine, which is directly converted from the on-site part of the power driving the machine. Similarly, $P_{drive,off}(t)$ is the off-site part of the heating power entering the thermal process of the machine, which is directly converted from the off-site part of the power driving the machine. Taking the GSHP in heating mode as an example, $P_{drive,on}(t)$ and $P_{drive,off}(t)$ are, respectively, equal to the on-site ($E_{on\text{-}h}(t)$) and off-site ($E_{off\text{-}h}(t)$) electrical power driving the compressor. $P_{amb}(t)$ is the "heating power" entering the thermal process of the machine from the ambient outside the boundary of the building. The ambient can be air, ground, lake or other elements. The underlying principle here is that we treat $P_{amb}(t)$ as the on-site heating power, such as heating power transferred from the ground to the evaporator of the GSHP in heating mode. It should be specifically mentioned that $P_{amb}(t)$ can only be the "heating power" instead of the "cooling power" entering the thermal process of the machine from the ambient outside the boundary of the building. Taking the GSHP in the cooling mode as an example, the "heating power" is transferred from the condenser to the ground; thus, there is no "heating power" entering the thermal process of the machine from the ground, i.e. $P_{amb}(t)$ is equal to zero in the cooling mode. This definition for $P_{amb}(t)$ is to make Equation (12) generalised and applicable to the special rule for the treatment of electrically or thermally driven cooling machine.

In addition, it should be mentioned that this thesis is only focused on the energy matching indices for evaluating the matching capability of the building energy systems with all energy forms, energy conversions, diversified storages and hybrid grid connections, whereas this thesis is not focused on evaluating the influence of the on-site energy systems on certain energy grid. The matching indices can not be used to exclusively evaluate the interactions between the on-site energy systems and certain energy grid. For example, neither "OEFh" nor "1-OEFh" can be generally used to show how much heating demand is covered by the heating grid, because the off-site heating can also be partly resulting from the imported electrical grid energy via the energy conversion processes. In order to show the exclusive influence of the on-site energy systems on the certain energy grid, grid interaction indices should be used, such as grid interaction index [27] and capacity factor [29]. They are reviewed and introduced in [28]. However, they are not the topic in this thesis.

Moreover, both the basic and extended matching indices are completely different from the so-called "Renewable Energy Ratio (RER)" defined in REHVA nZEB report [41] or PrEN 15603 [42]. It is important to distinguish between the RER and matching indices. The equation of RER has been shown below in Equation (13):

$$RER=\frac{\sum_i E_{ren,i}+\sum_i((f_{del,tot,i}-f_{del,nren,i})E_{del,i})}{\sum_i E_{ren,i}+\sum_i(f_{del,tot,i}E_{del,i})-\sum_i(f_{exp,tot,i}E_{exp,i})} \quad (13)$$

where $E_{ren,i}$ is the renewable energy produced on-site for energy carrier i; $E_{del,i}$ is the delivered energy to the building for energy carrier i; $E_{exp,i}$ is the exported energy from the building for energy carrier i; $f_{del,tot,i}$ is the total primary energy factor for the delivered energy carrier i; $f_{del,nren,i}$ is the non-renewable primary energy factor for the delivered energy carrier i; $f_{exp,tot,i}$ is the total primary energy factor for the exported energy carrier i. The energy carrier i in Equation (13) can represent the electrical, heating, and cooling energy forms. As shown in Equation (13), the basic principle for RER is to calculate the share of the renewable energy use in the total primary energy use in the building. Thus, its basic principle is different from the principles for the basic and extended matching indices. More specifically, the RER is based on the considerations of the primary energy use, whereas the basic and extended matching indices are focused on the direct energy use. Furthermore, RER is focused on the aspect of renewable energy, whereas the basic and extended matching indices are focused on the aspect of on-site energy: the on-site energy can contain both the renewable and non-renewable energy, while the renewable energy can contain both the on-site and off-site energy. In addition, although the concept of RER can also be used for each time-step, the main purpose is for calculating the annual renewable energy share as defined in [41] and [42]. However, the basic and extended matching indices can be used very flexibly for different periods with respect to certain designated time-step.

### 2.2.3 One time-step example for the usage of extended indices' equations

In order to briefly show the usage of extended indices' equations, an example of the matching situation for a PV-assisted ground source heat pump with electrical grid feed-in is presented in this section. The topology of the system is depicted in Figure 7, which is a specific simplification based on the general topology of Figure 4. The hybrid system is composed of a PV, a ground source heat pump (GSHP), and a heat storage. The PV is meant to meet all the electrical loads, including that of the GSHP. When the electrical power generated by the PV is insufficient in covering all the electrical loads, the electrical power is imported from the electrical grid to cover the shortage; when the electrical power generated by the PV is sufficient in meeting all the electrical loads, any surplus electrical power is exported to the electrical grid. Thus, two situations for one time-step are shown in this example, denoted by Situation 1 and Situation 2, with sufficient and insufficient solar radiation, respectively. The COP of GSHP in Situations 1 and 2 at this time-step are both equal to 3.0. It should be mentioned that the system shown in this simple example is to illustrate the usage of extended indices' equations when the system combination and control strategies are not optimised. With the specific topology of Figure 7, the equations for OEFe, OEFh, OEMe, and OEMh can be simplified, as listed in Equations (14)-(17):

$$\mathrm{OEFe} = \frac{\int_{t_1}^{t_2} \mathrm{Min}[G_{elec}(t) - l_e(t);\, L_{elec}(t) + E_{off\text{-}h}(t) + E_{on\text{-}h}(t)]dt}{\int_{t_1}^{t_2} [L_{elec}(t) + E_{off\text{-}h}(t) + E_{on\text{-}h}(t)]dt} \qquad (14)$$

$$OEFh = \frac{\int_{t_1}^{t_2} Min[H_{eon\text{-}h}(t) - HS_{on}(t) - l_h(t);\ L_{heat}(t)]dt}{\int_{t_1}^{t_2} L_{heat}(t)dt} \quad (15)$$

$$OEMe = \frac{\int_{t_1}^{t_2} Min[G_{elec}(t);\ L_{elec}(t)+E_{on\text{-}h}(t)+l_e(t)]dt}{\int_{t_1}^{t_2} G_{elec}(t)dt} \quad (16)$$

$$OEMh = \frac{\int_{t_1}^{t_2} Min[H_{eon\text{-}h}(t);\ L_{heat}(t)+HS_{on}(t)+l_h(t)]dt}{\int_{t_1}^{t_2} H_{eon\text{-}h}(t)dt} \quad (17)$$

***Situation 1***

In Situation 1, the electrical load (excluding the electrical load of the GSHP), $L_{elec}(t)$, and the heating load, $L_{heat}(t)$, are 2 kW and 5 kW, respectively, while the electrical load of the GSHP, i.e. '$E_{off\text{-}h}(t)+E_{on\text{-}h}(t)$', is 3 kW. The 12 kW of on-site PV power, $G_{elec}(t)$, is more than sufficient for meeting all of the electrical loads, including that of the GSHP; as a result, 4 kW of on-site electrical power is exported to the electrical grid. The electrical loss of on-site electrical power during the distribution, $l_e(t)$, is 3 kW, which is mainly due to the losses in the regulator and inverter. The values for OEFe and OEMe can be obtained using Equations (14) and (16). In Situation 1, the OEFe is 1.00, which indicates that all of the electrical loads, including that of the GSHP, are completely covered by the on-site PV production. As a result, the OEMe in Situation 1 is 0.67, which indicates that 67% of the generated on-site PV power is consumed in the building and system, while the remaining 33% of the power is fed to the electrical grid. For a GSHP with a COP of 3.0 and an electrical consumption of 3 kW, the evaporator absorbs 6 kW of heating power from the ground, which is the value for $P_{amb}(t)$ in Equation (12). The corresponding values of $H_{eon\text{-}h}(t)$ and $H_{eoff\text{-}h}(t)$ can be obtained using Equations (11) and (12); these values are presented in Figure 7(a). Due to the surplus of on-site renewable heating production, a net on-site heating power of 3.5 kW is charged to the heat storage. Moreover, the loss of on-site heating power during the distribution, $l_h(t)$, is 0.5 kW. As a result, the values of OEFh and OEMh are both 1.00 when using Equations (15) and (17), which indicates a perfect matching situation for the heating aspect.

***Situation 2***

In Situation 2, solar radiation is insufficient, while the load values of $L_{elec}(t)$ and $L_{heat}(t)$ are the same as in Situation 1. Moreover, the electrical load of the GSHP ('$E_{off\text{-}h}(t)+E_{on\text{-}h}(t)$') in Situation 2 is 1 kW. An inadequate PV production of 2 kW means that 1.5 kW of electricity needs to be imported from the electrical grid. The electrical loss of on-site electrical power during the distribution, $l_e(t)$, is 0.5 kW. By Equations (14) and (16), the values of OEFe and OEMe are 0.50 and 1.00, respectively, indicating that half of the overall electrical loads including that of the GSHP are covered by the on-site PV production, and that all of the generated PV power is completely consumed in the building and system. Since

the OEFe is equal to 0.5, $E_{off\text{-}h}(t)$ and $E_{on\text{-}h}(t)$ are both the same at the value of half the GSHP electrical consumption. For a GSHP with a COP of 3.0 and an electrical consumption of 1 kW, the evaporator absorbs 2 kW of heating power ($P_{amb}(t)$ in Equation (12)) from the ground. The calculated $H_{eon\text{-}h}(t)$ and $H_{eoff\text{-}h}(t)$ are 2.5 kW and 0.5 kW, respectively, when using Equations (11) and (12). The net heating power discharged from the heat storage is 2.2 kW. The ratio of the stored on-site heating to the off-site heating energy in the heat storage is based on the charging and discharging of the heat storage from the initial operation of the whole system. Here, it is simply assumed that at the current time-step, the net discharged heating power of 2.2 kW consists of 1.9 kW of on-site heating power and 0.3 kW of off-site heating power. Moreover, $l_h(t)$ is 0.2 kW. The values of OEFh and OEMh are obtained when using Equations (15) and (17). The OEFh is 0.84, which indicates that 84% of the heating load is covered by the on-site renewable heating production, while OEMh is still at a value of 1.00. Since no heating grid is available, all of the generated on-site renewable heating power is entirely consumed in the building and system, which is the reason for the OEMh unity in both Situations 1 and 2. Furthermore, there is a much higher OEFh than OEFe in Situation 2, which is due to the heating power absorbed by the evaporator from the ground and the net on-site part of the heating power discharged from the heat storage.

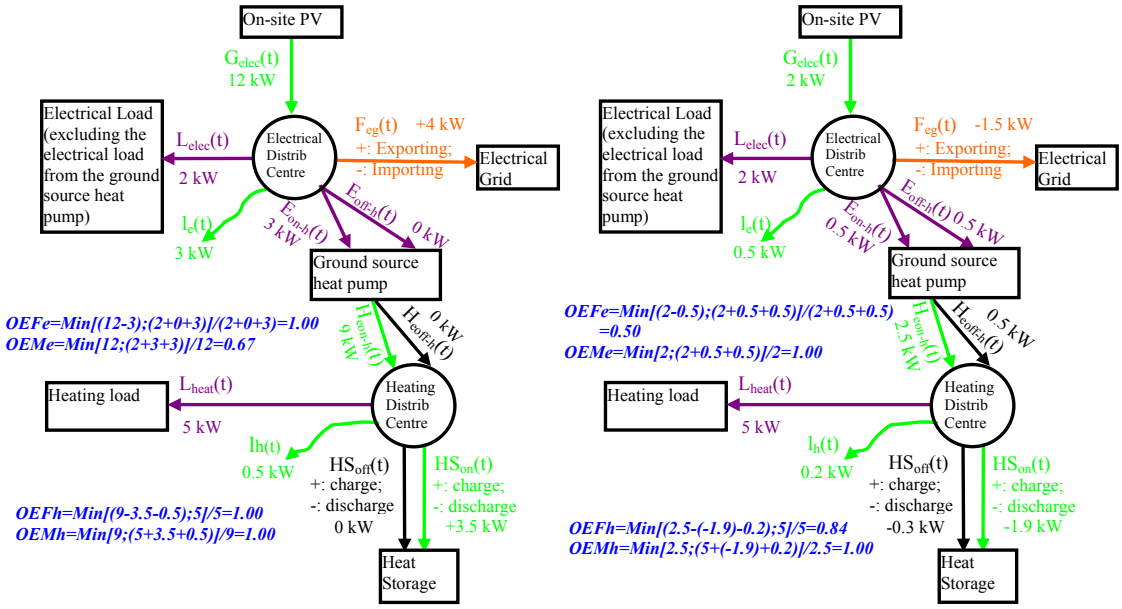


Figure 7. The topologies of the on-site matching indices for (a) Situation 1, and (b) Situation 2. The power values shown in the diagram are for one time-step.

## 2.3 Further extension of the own-defined topology and indices

The topology shown in Figure 4 can also be extended to some very special applications. For example, if the electrically

driven heating machine is a heat pump in heating mode, the cooling power generated by the evaporator of the heat pump might be simultaneously utilised. Similarly, the heating power generated from the condenser of the electrically or thermally driven cooling machines might also be simultaneously utilized. Under these special situations, as shown in Figure 8, there will be two more additional lines, one for the on-site ("$C_{eon\text{-}h}(t)$") and the other for the off-site ("$C_{eoff\text{-}h}(t)$"), connecting from "electrically driven heating machines" to the "cooling distribution centre"; similarly, there will be two additional arrow lines ("$H_{eon\text{-}c}(t)$" and "$H_{eoff\text{-}c}(t)$") connecting from "electrically driven cooling machines" to the "heating distribution centre", and two additional arrow lines ("$H_{hon\text{-}c}(t)$" and "$H_{hoff\text{-}c}(t)$") connecting from "thermally driven cooling machines" to the "heating distribution centre". These additional arrow lines are depicted in Figure 8 by black (representing off-site power) or green (representing on-site power) colour, while the existing arrow lines referring to Figure 4 are depicted with grey colour. Regarding the nomenclature, $C_{eon\text{-}h}(t)$ and $C_{eoff\text{-}h}(t)$ are the simultaneous cooling powers generated by the evaporator of the electrically driven heating machine by the on-site and off-site part of the driving electricity, respectively; $H_{eon\text{-}c}(t)$ and $H_{eoff\text{-}c}(t)$ are the simultaneous heating powers generated by the condenser of the electrically driven cooling machine by the on-site and off-site part of the driving electricity, respectively; $H_{hon\text{-}c}(t)$ and $H_{hoff\text{-}c}(t)$ are the simultaneous heating powers generated by the condenser of the thermally driven cooling machine by the on-site and off-site part of the heat, respectively. These terms can be added to the Equations (5)-(10) with the same principle described in Section 2.2.2. Furthermore, under these special situations, according to the author's own point of view, the on-site proportion of the generated heating or cooling powers by the conversion machines should still follow the calculation method presented in Equation (12). $P_{amb}(t)$ should still be equal to the "heating power" transferred from the ambient outside the boundary to the machine. Under the very special situations that the cooling power generated by the evaporator and the heating power generated by the condenser can both be fully utilised, the $P_{amb}(t)$ in Equation (11) will become zero, because there is no "heating power" transferred from the ambient outside the boundary to the machine (the evaporator absorbs the heating power from the space inside the boundary of the building).

Due to rare occurrence of these special situations, the generalised topology in the following sections will still be according to the topology of Figure 4 to avoid excessive complexity, that would result from additional arrow lines, in the illustration.

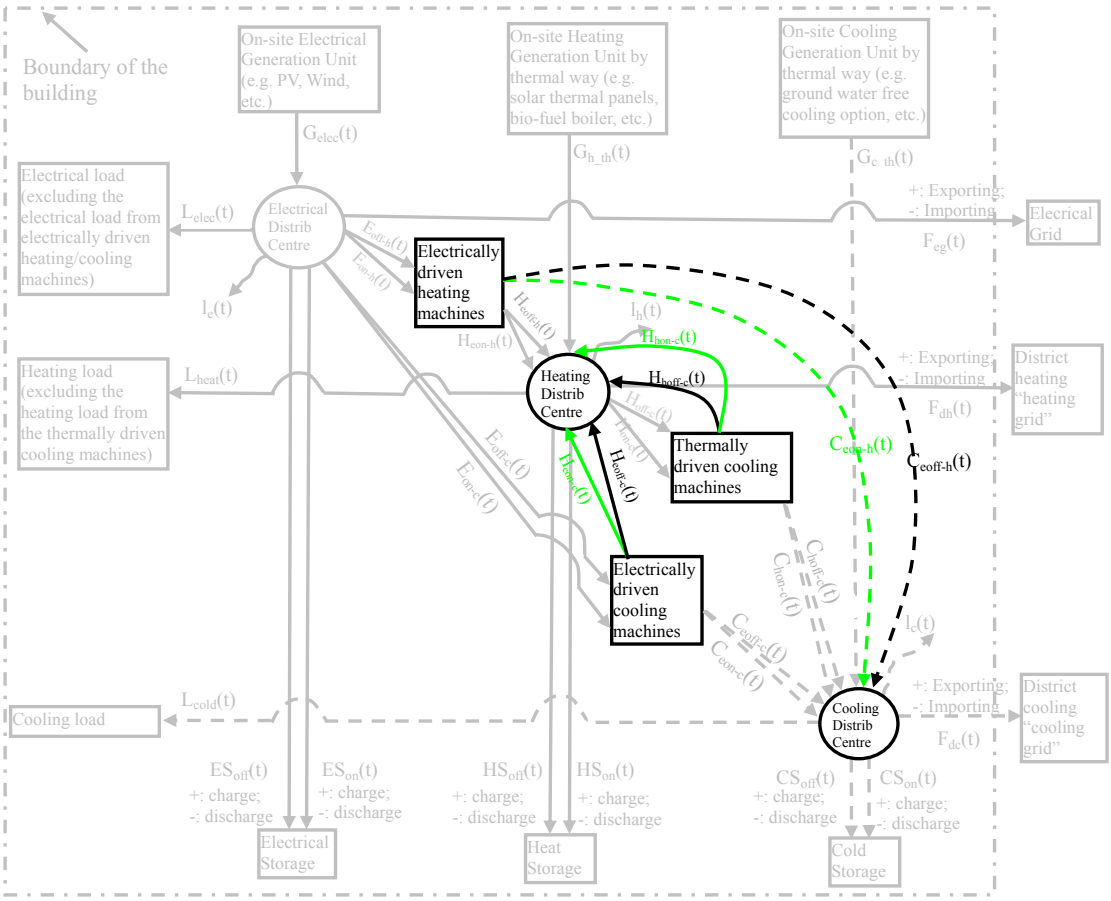


Figure 8. The extension of the topology under special situations. The additional arrow lines are depicted with black (representing off-site power) or green (representing on-site power) colour while the existing arrow lines referring to Figure 4 are depicted with grey colour.

# 3 Implementation of indices

## 3.1 Diversified treatments of excess on-site energy production (Original publications I, II and III)

Due to energy conversions, various energy storages and hybrid grid connections, the handling methods of excess on-site energy generation are diversified. Generally speaking, there are six options:

(1) Allocation of excess on-site production for the fulfilment of on-site energy demand with the same energy form, e.g. allocation of the excess on-site electrical production generated by PV for the fulfilment of the electrical demand of the lights;

(2) Allocation of excess on-site production for the charge of energy storage with the same energy form, e.g. allocation of the excess on-site electrical production generated by PV for the charge of an electrical battery;
(3) Allocation of excess on-site production for distributed feed-in of a certain energy grid (electrical, heating, or cooling grid) with the same energy form, e.g. allocation of the excess on-site thermal heating production generated by solar thermal collectors for the distributed feed-in of the heating grid;
(4) Re-allocation of excess on-site production for the fulfilment of on-site energy demand with different energy forms through energy conversion processes, e.g. re-allocation of the excess on-site electrical production generated by PV for the fulfilment of the heating demand through electrical heater;
(5) Re-allocation of excess on-site production for the charge of an energy storage with different energy forms through energy conversion processes, e.g. re-allocation of the excess on-site thermal heating production generated by parabolic solar thermal collectors for the charge of the cold storage through a solar thermal driven absorption chiller;
(6) Re-allocation of excess on-site production for distributed feed-in of a certain energy grid (electrical, heating, or cooling grid) with different energy forms through energy conversion processes, e.g. re-allocation of the excess on-site electrical production generated by PV for the distributed feed-in of the heating grid through an electrical heater.

All the aforementioned options can be depicted in the topology of Figure 4 for the comprehensive matching analysis. Due to the existence of the abovementioned diversified options, it will be much more sophisticated for the analysis and design of future on-site energy systems involving all energy forms, energy conversions, various storage types and hybrid grid connections. In the following Section 3.2, the design and analysis of hybrid on-site renewable energy systems, from the standpoint of matching, will be carried out, with the aid of the extended matching indices and the topology, for two office buildings.

## 3.2 Matching indices for aiding the design of the office system (Original publication III)

### 3.2.1 Simulation environment, climate, and building parameters

The analysis and the design of office buildings are conducted in a dynamic numerical simulation environment — TRNSYS 17 [43]. The selected time-step is 15 minutes, which indicates that the data of on-site generated and demand powers are both averaged over 15 minutes time-step. However, in practice, both are instantly variable. Therefore, the selection of the time-step essentially contains a presumption that there is a short-term energy buffer to level off the power fluctuations within 15 minutes. Actually, for the heating and cooling aspects, the presumption of 15 minutes buffer is not necessary due to the existence of the heat and cold storages, which are obligatory in the latter introduced

systems. These thermal storages are with enough thermal capacity to level off the fluctuations of thermal heating and cooling powers within 15 minutes. Regarding the electrical aspect, the presumption of 15 minutes buffer is meaningful, because in the later analysis there are cases with no battery. And it contains the presumption that the capacity of the 15-minute electrical buffer is much smaller than that of any battery size with non-zero capacity considered in the latter analysis.

In order to show the general applicability of the methodology of matching analysis with extended matching indices, the selected locations are based on the consideration of distinct climate conditions. Therefore, two office buildings are selected for the analysis, one in Helsinki with heating-dominant characteristics and one in Shanghai with cooling-dominant characteristics. The weather files are taken from the TRNSYS standard TMY2 files for Helsinki and Shanghai [43]. The integrated annual weather conditions generated from these weather files are listed in Table 2. The two buildings are both two-storey office buildings and share the same layout plans and orientations, as shown in Figure 9. The parameters of envelopes and infiltrations are listed in Table 2. The internal shadings are used for the windows of both office buildings. In Helsinki, the internal shading is used from June 1st to August 31st, and, in Shanghai, from May 15th to September 30th. The internal shading factors of both office buildings also follow a 15-minute time-step profile defined by the author. The parameters of the ventilation systems strictly follow the regulations defined in the Finnish Building Regulation D3 [44] and the Chinese Public Building Regulation GB 50189-2005 [45]. In Helsinki, mixing of fresh supply air and exhaust air is not allowed [44], instead a totally fresh air supply is used for the ventilation system, i.e. the fresh air ratio is equal to 1. In Shanghai, the fresh air ratio is regulated according to [45], regarding the occupancy density and the ventilation flow rates. Both the specific fan powers of supply and exhaust fans have the value of 1000 $W/(m^3/s)$ in Helsinki [44], and both have the value of 1512 $W/(m^3/s)$ in Shanghai [45]. Both of the two office buildings are equipped with a rotary heat recovery system; the annual sensible efficiency of the rotary heat recovery system is at 0.85, while the exhaust air temperature is higher than -5 °C [44].

The occupancies and internal gains follow the regulations defined in [44] and [45] for Helsinki and Shanghai, respectively. In Helsinki, the number of occupants in the office cell, open-plan office, and meeting room are 1, 12, and 5, respectively, while in Shanghai, the corresponding values are 1, 19, and 9, respectively. Each occupant has an activity level of 1.2 MET [46]. The attendance profiles of the occupants in the office cell and open-plan office follow the profiles obtained from [47] and [45] for Helsinki and Shanghai, respectively. The attendance profiles in the meeting room have not been defined in [44], [47] and [45]; thus an assumption is made for both office buildings that the attendance profile is 100% from 9:00 to 11:00 and from 14:00 to16:00, while the value is 0% for the rest of the hours. The consumption

profiles of lightings and appliances in the Helsinki office building are achieved from [47], which is further scaled to fit the annual consumption figures defined in [44], whereas the consumption profiles of lightings and appliances in the Shanghai office building are directly obtained from [45]. As a result, the annual internal gains, annual consumption of lighting, and annual consumption of appliances in Helsinki are 15.5 kWh/m$^2$ a, 22.4 kWh/m$^2$ a, and 22.4 kWh/m$^2$ a, respectively, while the corresponding values in Shanghai are 33.3 kWh/m$^2$ a, 33.2 kWh/m$^2$ a, and 21.1 kWh/m$^2$ a, respectively.

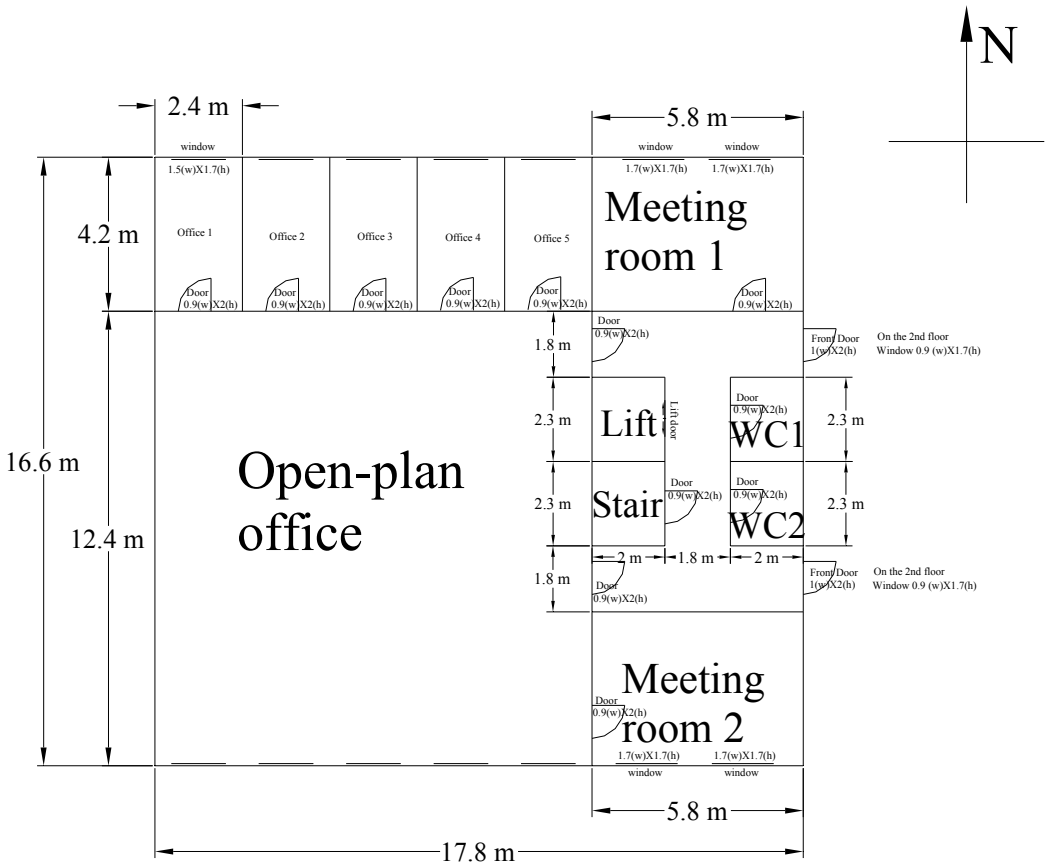

Figure 9. The brief plan of office building [Original publication III].

Table 2. The climate, U values, and infiltration of the two office buildings [Original publication III].

| | | Helsinki [44] | Shanghai [45] |
|---|---|---|---|
| Climate | Annual dry bulb temperature (°C) | 4.7 | 15.8 |
| | Annual heating degree days (base temperature 18 °C) | 4878 | 1868 |
| | Annual cooling degree days (base temperature 18 °C) | 32 | 1056 |
| | Annual overall solar radiation on horizontal surface (kWh/m$^2$ a) | 969 | 1314 |
| U-values (W/m$^2$ K) | External wall | 0.166 | 0.995 |
| | External roof | 0.089 | 0.685 |
| | Adjacent ceiling | 1.353 | 1.353 |
| | Partition wall | 0.474 | 1.282 |
| | External window | 0.98 | 2.83 |
| | Front door | 0.98 | 2.83 |
| | Ground floor layer | 0.116 | 0.718 |
| | 1 m Soil layer below the ground floor layer | 1.493 | 1.493 |
| Infiltration (ACH) | | 0.045 | 0.2 |

### 3.2.2 Heating and cooling systems

The AHU heating and cooling are realised through hydronic heating and cooling coils. For both the office buildings in Helsinki and Shanghai, 40/30 °C underfloor heating is adopted for space heating, while the chilled beam is adopted for space cooling. The supply heat transfer fluid temperatures for AHU and space cooling are 7 °C and 15 °C, respectively. The set point for domestic hot water (DHW) is 55 °C, while the temperatures of inlet cold city water before heating are 5 °C and 7 °C in Helsinki and Shanghai, respectively. The daily volume consumptions of DHW in the Helsinki and Shanghai office buildings are 233 L/day [44] and 363 L/day during the weekdays, respectively. The set point temperatures of room air are set according to [44] and [45]. Table 3 lists the annual overall heating and cooling demands, from which it can be seen that the Helsinki office has a heating-dominant thermal demand whereas the Shanghai office has a cooling-dominant thermal demand.

Table 3. The annual heating and cooling demands [Original publication III].

| | Heating demand (kWh/m$^2$ a) | | | | Cooling demand (kWh/m$^2$ a) | | |
|---|---|---|---|---|---|---|---|
| | AHU heating | Space heating | DHW heating | Sum | AHU cooling | Space cooling | Sum |
| Helsinki | 16.9 | 13.0 | 6.0 | 35.9 | 2.3 | 7.7 | 10 |
| Shanghai | 4.5 | 22.3 | 9.0 | 35.8 | 109.0 | 7.6 | 116.6 |

The heating and cooling systems of the two office buildings follow a similar system configuration as shown in Figure 10. The system configurations differ in that the system in Helsinki should exclude the part enclosed by the pink long centre

line, whereas the system in Shanghai should exclude the part enclosed by the blue long dashed line. As shown in Figure 10, the system is a solar assisted ground source heat pump (GSHP). The parameters of the GSHP, heat transfer fluid, storage tanks, ground boreholes, and ground in Helsinki and Shanghai are listed in Table 4.

The GSHP can work either in a heating or in cooling mode, and the switch strategy between these modes is as follows: when the average HTF temperature in tank C2 is higher than 6.5 °C, the GSHP operates in the cooling mode; for the rest of the time, it operates in the heating mode. A temperature level of 40-45 °C is kept in tank H1 for the DHW, AHU and space heating purposes. Without any solar (PV or solar thermal) assisted system, more than 90% (94.4% in Helsinki and 93.8% in Shanghai) of the overall heating demands can be covered by the GSHP with tank H1. The rest of the heating demands is due to three reasons: (1) the set point temperature in tank H1 is kept at the level of 40-45 °C, which is lower than the set point temperature of DHW at 55 °C; (2) the instantaneous heating demand peak; (3) the switch strategy between the heating and the cooling mode for the GSHP determines that when the cooling mode is in operation, the heating mode should be terminated – this problem, however, is minor, because it occurs mainly in the summer and late spring when the heating demands are low. Thus, in order to meet the entire heating demands, the auxiliary heating devices should be equipped as shown in Figure 10. Regarding certain control strategies introduced in the latter Section 3.2.4, the auxiliary heating devices are realised either by electrical heaters or the heating grid.

In the system of Helsinki office building, the tanks C1 and C2 are both equipped. Tank C1 is charged by a free ground cooling option to maintain the temperature level between 13 and 14.5 °C. Tank C2 is charged by the GSHP in cooling mode to maintain the temperature level between 5 and 6.5 °C. The AHU cooling demand can be entirely met by extracting the cooling from tank C2. Moreover, the HTF of space cooling firstly flows through tank C1; if the set point is not met by flowing through tank C1, the HTF will be sent to flow through tank C2. No auxiliary cooling device is required in the Helsinki office building, which is the reason why the part enclosed by the pink long centre line is excluded in the Helsinki office system, as shown in Figure 10. In the Shanghai office building, there is no free ground space cooling or tank C1, because the ground temperature (Table 4) is not suitable for meeting the set point of space cooling, which is also the reason why the part enclosed by the blue long dashed line is excluded in the Shanghai office system, as shown in Figure 10. Furthermore, due to the instantaneous AHU cooling power in Shanghai, 7.2% of the overall cooling demands can not be met by the GSHP with tank C2. Thus, an auxiliary cooling device should be equipped for the AHU cooling in the Shanghai office building, while the realisation method can be either an auxiliary refrigeration chiller (average COP of 2.0) or the cooling grid, regarding certain control strategies introduced in the latter Section 3.2.4. It should additionally be mentioned that there is currently no heating or cooling grid available in Shanghai.

The optional inclusion of the heating and cooling grids in the system is for the research purposes for the comparison with the system in Helsinki. The author of this thesis believes that in the future, the hybrid grid networks of electrical, heating, and cooling will be successfully accomplished in the urban area of Shanghai as those developed in the Helsinki urban area.

When a solar thermal system is included for aiding the GSHP, tank H2 will be used. As shown in Figure 10, the solar thermal collectors can charge both tanks H2 and H1. The solar thermal collectors first charge tank H2. Thereafter, when the HTF temperature at valve V7 is higher than the top node temperature of tank H1, it will flow through valve V8 to charge tank H1; otherwise, it will flow through valve V9. The valves V13-V18 are used for heating grid feed-in option, which is introduced in the latter Section 3.2.4.

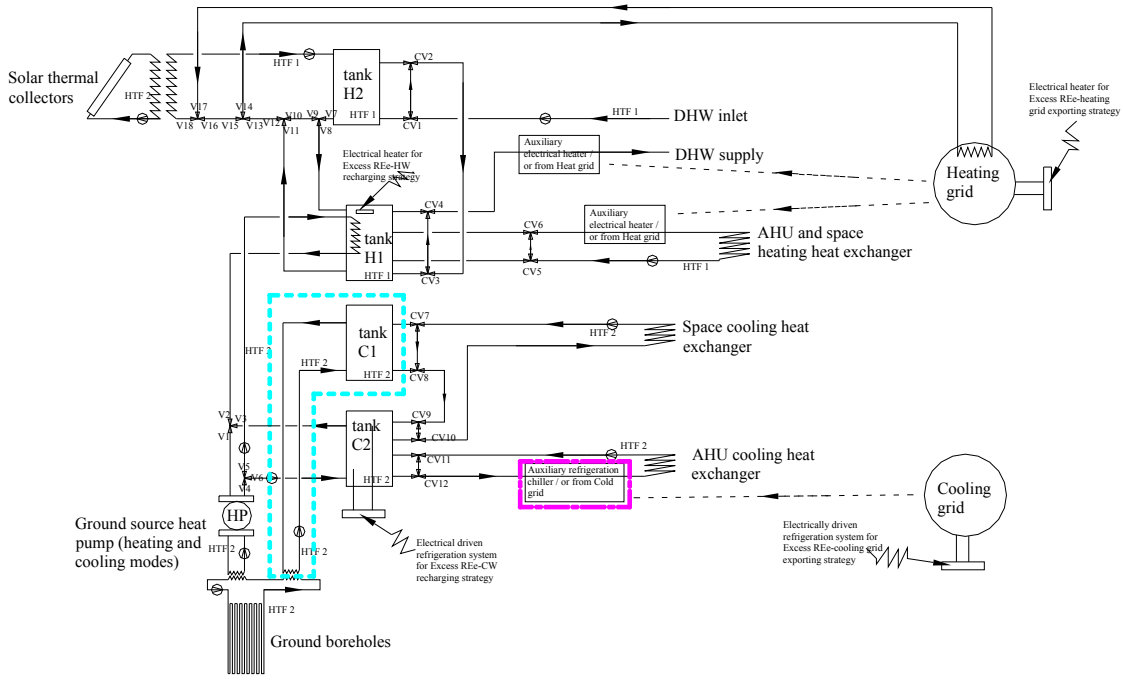


Figure 10. The heating and cooling system for the office building. For the Helsinki office building, the system excludes the part enclosed by pink long centre line; for the Shanghai office building, the system excludes the part enclosed by blue long dash line. HTF 1: water; HTF 2: 33%Vol propylene glycol in Helsinki, or 25%Vol propylene glycol in Shanghai. [Original publication III]

Table 4. The parameters of ground source heat pump, heat transfer fluid, thermal storage tanks, ground boreholes, and ground [Original publication III].

| | Helsinki | Shanghai |
|---|---|---|
| Ground source heat pump | Carrier® 50PSW180 [48]<br>(Nominal heating capacity: 28.9 kW<br>Nominal cooling capacity: 36.8 kW<br>Nominal COP of heating: 3.2<br>Nominal COP of cooling: 5.0)[(a)] | Carrier® 50PSW360 [48]<br>(Nominal heating capacity: 57.3 kW<br>Nominal cooling capacity: 73.8 kW<br>Nominal COP of heating: 3.2<br>Nominal COP of cooling: 5.0)[(a)] |
| Heat transfer fluid | HTF1: water<br>HTF2: 33%Vol propylene glycol | HTF1: water<br>HTF2: 25%Vol propylene glycol |
| Size of thermal storage tanks (Vertical cylinder) | Tank H1: 2 $m^3$ volume, 1.37 m height;<br>Tank H2: 0.25 $m^3$ volume, 0.68 m height;<br>Tank C1: 1 $m^3$ volume, 1.08 m height;<br>Tank C2: 1$m^3$ volume, 1.08 m height. | Tank H1: 2 $m^3$ volume, 1.37 m height;<br>Tank H2: 0.25 $m^3$ volume, 0.68 m height;<br>Tank C1: non-existent<br>Tank C2: 2 $m^3$ volume, 1.37 m height. |
| Ground boreholes | Borehole type: Single U-tube boreholes<br>Number of boreholes: 9<br>Borehole diameter: 152.4 mm<br>Borehole depth: 134 m<br>Borehole spacing: 7 m<br>Borehole filling material: Sand moist (thermal conductivity is 1.3 W/m K)<br>Outlet diameter of U-tube pipe: 40 mm<br>Wall thickness of U-tube pipe: 2.3 mm<br>Thermal conductivity of U-tube pipe: 0.42 W/m K<br>Shank spacing of U-tube pipe: 100 mm | Borehole type: Single U-tube boreholes<br>Number of boreholes: 16<br>Borehole diameter: 152.4 mm<br>Borehole depth: 180 m<br>Borehole spacing: 12 m<br>Borehole filling material: Sand moist (thermal conductivity is 1.3 W/m K)<br>Outlet diameter of U-tube pipe: 40 mm<br>Wall thickness of U-tube pipe: 2.3 mm<br>Thermal conductivity of U-tube pipe: 0.42 W/m K<br>Shank spacing of U-tube pipe: 100 mm |
| Ground | Ground type: Granite<br>Thermal conductivity: 3.4 W/m K<br>Volumetric heat capacity: 2.4 $MJ/m^3$ K<br>Undisturbed ground temperature: 7 °C [49] | Ground type: Silt<br>Thermal conductivity: 1.8 W/m K<br>Volumetric heat capacity: 2.2 $MJ/m^3$ K<br>Undisturbed ground temperature: 18 °C [50] |

(a) Nominal heating conditions: indoor entering water temperature of 40 °C, outdoor entering water temperature of 0 °C; nominal cooling conditions: indoor entering water temperature of 12 °C, outdoor entering water temperature of 25 °C [48].

### 3.2.3 The specifications of solar system (PV and solar thermal collectors)

The REe system used in this office building is a PV system. The geometrical positions of PV panels are chosen at a value of 45° tilted angle due south in both Helsinki and Shanghai, according to the proposed values suggested by the IEA PV Manual [51] to achieve the maximum annual received solar radiation. This geometrical position is also supported by the simulation results of TRNSYS 17. With the same reason, all the solar thermal collectors are also with 45° tilted angle due south in both Helsinki and Shanghai office buildings.

The PV system contains multiple PV modules, each with a nominal power of 0.10 kW and an area of 0.89 $m^2$. The annual efficiency of the PV module at the maximum power point (MPP) is around 11% [43]. The number of modules is one of the analysed parameters in the latter Section 3.2.5, thus is not presented here. The detailed technical parameters of the PV module are listed in Table 5. The solar thermal collectors are also composed of multiple collector modules, each with a surface area of 3 $m^2$. The number of connection modules and connection types are one of the analysed parameters

in the latter Section 3.2.5, thus are not presented here. The detailed technical parameters of the solar thermal collector module are listed in Table 6.

Table 5. The parameters of the PV system set in the TRNSYS simulation.

| Parameter | Value |
|---|---|
| The type used in TRNSYS 17 | Type 194 [43] |
| Module short-circuit current at reference conditions (Ampere) | 6.5 |
| Module open-circuit voltage at reference conditions (V) | 21.6 |
| Reference temperature (K) | 298 |
| Reference insolation ($W/m^2$) | 1000 |
| Module voltage at maximum power point and reference conditions (V) | 17 |
| Module current at maximum power point and reference conditions (Ampere) | 5.9 |
| Temperature coefficient of Isc (reference condition) | 0.02 |
| Temperature coefficient of Voc (reference condition) | -0.079 |
| Number of cells wired in series | 36 |
| Number of modules in series | 2 |
| Number of modules in parallel | Case-dependent |
| Module temperature at nominal operating cell temperature (K) | 313 |
| Ambient temperature at nominal operating cell temperature (K) | 293 |
| Insolation at nominal operating cell temperature ($W/m^2.K$) | 800 |
| Area of each module ($m^2$) | 0.89 |
| Transmittance-absorptance product for normal incidence | 0.95 |
| Semiconductor bandgap | 1.12 |
| Value of parameter a at reference conditions | 1.9 |
| Value of parameter I_L at reference conditions (Ampere) | 5.4 |
| Value of parameter I_0 at reference conditions (Ampere) | 0 |
| Module series resistance | 0.5 |
| Shunt resistance at reference conditions | 16 |
| Extinction coefficient-thickness product of cover | 0.008 |

Table 6. The parameters of the solar thermal collector unit set in TRNSYS simulation. The technical data of solar thermal collector refers to the product of Clearline® V30 [52].

| Parameter | Value |
|---|---|
| The type used in TRNSYS 17 | Type 1a [43] |
| Each collector absorber area ($m^2$) | 3 |
| Intercept efficiency | 0.81 |
| Efficiency slope (kJ/hr $m^2$ K) | 14.04 |
| Efficiency curvature (kJ/hr $m^2$ $K^2$) | 0.032 |
| Mass flow rate of HTF through each collector module (kg/s) | 0.044 |

### 3.2.4 Excess renewable energy treatment strategies

As mentioned in Section 3.1, due to the existence of energy conversions, various storage types and hybrid grid networks, the treatments of the excess renewable energy production are much diversified. For the studied office buildings in Helsinki and Shanghai, there are six excess REe treatment strategies. Three of these strategies are for excess REe-thermal recharging:

(1) No excess REe-thermal recharging.

(2) Excess REe-hot water (excess REe-HW) recharging: the excess REe is used to recharge hot water storage tank H1

via an electrical heater, as shown in Figure 10, while the maximum allowed top node temperature of this tank H1 by this recharging method is 90 °C.

(3) Excess REe-cold water (excess REe-CW) recharging: the excess REe is used to recharge cold water storage tank C2 via an electrically driven refrigerator chiller (with average COP equal to 1.5 and 1.0 for Helsinki and Shanghai, respectively), while the minimum allowed bottom node temperature of tank C2 by this recharging temperature is -5 °C.

It should additionally be mentioned that, for simplification in this thesis, these three excess REe-thermal recharging strategies can not be simultaneously used in one year's simulation. The simultaneous use of these recharging strategies would need the study for the multi-objective optimization controls, which is not the main research theme in this thesis. Furthermore, in order to facilitate the understanding of these excess REe-thermal recharging strategies, Figure 11 presents the topology with highlighted portions referring to the excess REe-HW or excess REe-CW recharging strategy.

The remaining three strategies are for excess REe-grid exporting:

(1) Excess REe-electrical grid exporting: the excess REe is fed to the electrical grid. When this exporting strategy is activated, the auxiliary heating devices for AHU, space and DHW heating must be merely via the auxiliary electrical heaters; meanwhile, the auxiliary cooling device for AHU cooling must be merely via the auxiliary electrically driven chiller.

(2) Excess REe-heating grid exporting: the excess REe is fed to the heating grid (e.g. a district heating system) via the electrical heater. When this exporting strategy is available, the auxiliary heating devices for AHU, space and DHW heating must be merely via the heating grid, while the auxiliary cooling device for AHU cooling must be merely via the auxiliary electrically driven chiller.

(3) Excess REe-cooling grid exporting: the excess REe is fed to the cooling grid (e.g. a district cooling system) via the electrically driven chiller (with average COP equal to 2.5 and 2.0 for Helsinki and Shanghai, respectively). When this exporting strategy is available, the auxiliary heating devices for AHU, space and DHW heating must be merely via the auxiliary electrical heaters, while the auxiliary cooling device for AHU cooling must be merely via the cooling grid.

It should additionally be mentioned that, for simplification in this thesis, these three excess REe-grid exporting strategies can not be simultaneously used in one year's simulation. The simultaneous use of these exporting strategies would need the study for the multi-objective optimization controls, which is not the main research theme in this thesis. Moreover, in order to facilitate the understanding of these excess REe-grid exporting strategies, Figure 12 presents the topology with highlighted portions referring to the three excess REe-grid exporting strategies.

Furthermore, when the excess REe-heating grid exporting is available, the excess renewable thermal (REth)-heating grid

exporting should be used simultaneously. The control strategy of excess REth-heating grid exporting is explained as follows: if the HTF temperature at valve V13 is higher than 70 °C, the excess solar thermal energy will be fed to the heating grid via valve V14, and the return HTF temperature at valve V17 will be assumed to be at 70 °C; otherwise, the HTF will flow through valve V15 without feeding the heat into the heating grid. This simplified treatment is just for testing the matching indices. The technology of "Feed-in return→return", as one of the three main thermal feed-in technologies introduced in [53], can be adopted for the exportation of heat for this excess REth-heating grid exporting strategy at this medium temperature level higher than 70 °C.

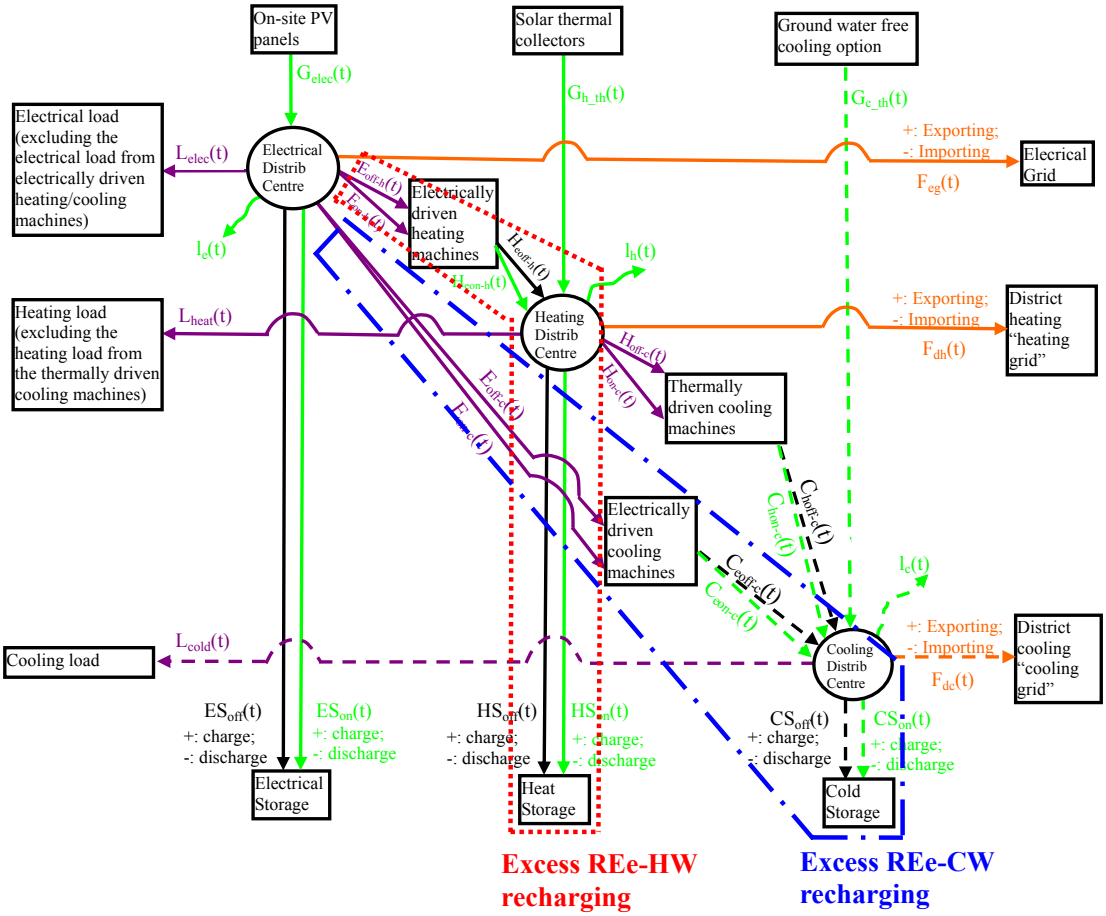


Figure 11. The topology referring to the excess REe-HW or excess REe-CW recharging strategy.

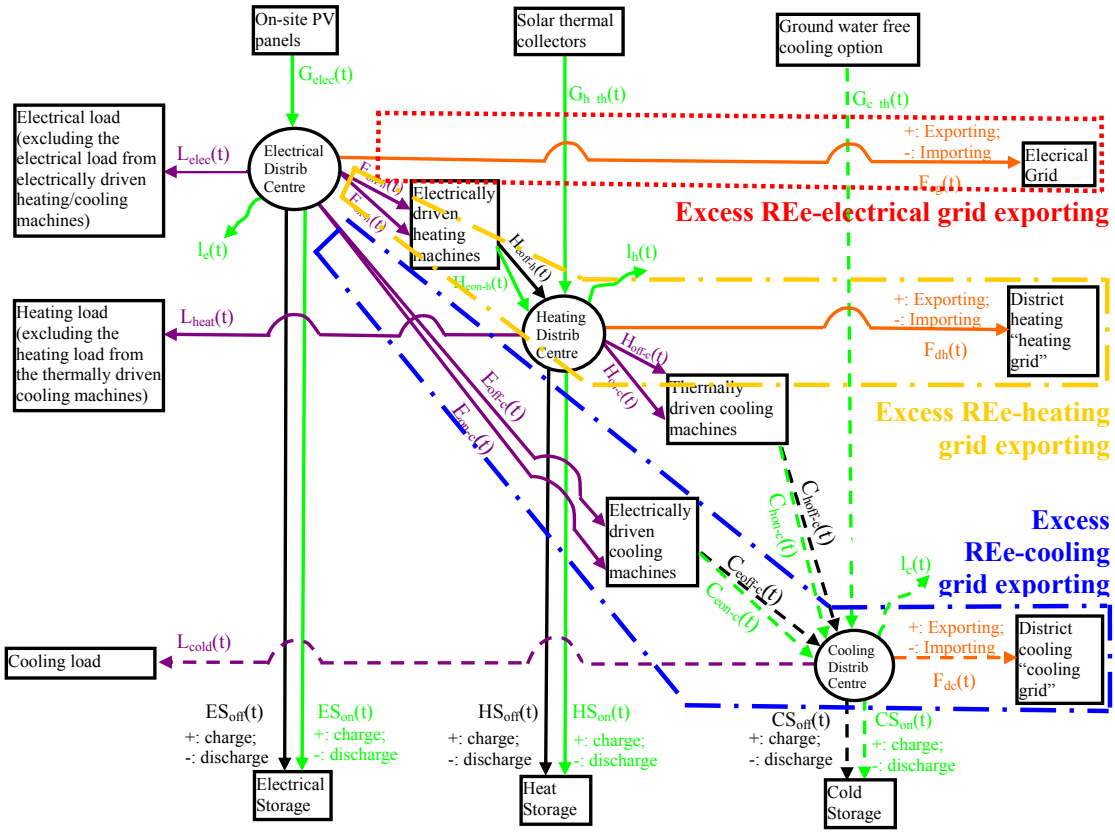


Figure 12. The topology referring to the excess REe-grid exporting strategies.

### 3.2.5 Parametric analysis of system components from matching aspect

#### 3.2.5.1 Solar thermal collector

The first analysed system component is the solar thermal system. The analysed variables include the connection type, solar thermal collector area, and exporting strategy. All the options of the variables are listed in Figure 8. Furthermore, it should be mentioned that there is no PV or battery system in the system. All the combinations of the options are analysed in the simulation. The connection Type 1 means that all the solar thermal collector modules are connected in series; the connection Type 2 is of the "3×n type", which means that the solar thermal collectors are connected creating n parallel lines, each line consisting of three series-connected modules. Figure 13 and Figure 14 present the annual energy matching results from the heating aspect under the connection types Type 1 and Type 2 ("3×n type"), respectively, with respect to the total collector areas and exporting strategies.

There are several important points to be aware of. Firstly, as shown in Figure 13 and Figure 14, the OEF values are higher than 0.65 in both Helsinki and Shanghai even if there is no solar thermal collector in the heating system. This is due to the on-site renewable heating absorbed from the ground to the evaporator of the heat pump.

Secondly, comparison between Figure 13 and Figure 14 shows the drawbacks of pure series connection and the advantages of the connection type "3×n type". On one hand, as shown in Figure 13 for the connection Type 1, the increase ratios of OEFh curves start to slow down from around 10 $m^2$ in both Helsinki and Shanghai. The saturated OEFh values with the connection Type 1 are around 0.8 and 0.74 in Shanghai and Helsinki, respectively. On the other hand, as shown in Figure 14 for the connection Type 2, the increase ratios of OEFh curves start to slow down from around 36-54 $m^2$ in both Helsinki and Shanghai, while the saturated OEFh values with the connection Type 2 are around 0.9 and 0.8 in Shanghai and Helsinki, respectively. The lower matching performance of OEFh with the connection Type 1 results from the shortage of the all series connection manner. Under the all series connection manner, the increase of collector module numbers leads to a continuous increase of the heat transfer fluid outlet temperature and a dramatic decrease in collector efficiency. Moreover, the control of the solar thermal cycle determines that when the outlet temperature of the solar collectors is higher than 90 °C, the solar thermal cycle should be turned off. Therefore, the useful solar thermal gain by the connection Type 1 is significantly limited compared to that by the connection Type 2, also making the heat exportation meaningless. This limitation can be well overcome by using the connection Type 2, because the connection manner of the "3×n type" avoids the undesirable increase of outlet temperature with respect to the increase of overall collector areas.

Thirdly, compared between the conditions with and without excess REth-heating grid exporting strategies, the main difference happens to the OEMh curves in Figure 14 with connection type 2. The difference regarding the excess REth-heating exporting strategies is negligible with the connection Type 1 because the heat exportation of this connection type is meaningless, as mentioned in the second point above. For the connection Type 2, when there is no excess REth-heating grid exporting, the OEMh values are both at unity under Helsinki and Shanghai conditions, because no solar thermal heating is dumped or exported. However, when the excess REth-heating grid exporting is activated, the OEMh curves continuously decrease with respect to the increase of total solar thermal collector areas, indicating effective heat exportation to the heating grid. Within the range of 36-54 $m^2$, where the increase ratio of the OEFh curves starts to slow down, the OEMh values in Helsinki and Shanghai are both higher than 0.8, indicating good OEFh and OEMh matching situations. Thus, in the following sections, whenever solar thermal collectors are used, an area value of 45 $m^2$ is chosen for them in both Helsinki and Shanghai. The corresponding OEFh and OEMh values are 0.77 and 0.88

in Helsinki, respectively, while in Shanghai they are 0.86 and 0.82, respectively.

Table 7. The options of connection type, collector area and exporting strategy [Original publication III].

| | Options |
|---|---|
| Connection type | Type 1: All connected in series<br>Type 2: "3×n type" |
| Total solar thermal collector area ($m^2$) | For Connection Type 1: 0, 3, 6, 9, 12, 15, 21, 27, 33, 39, 45, 51<br>For Connection Type 2: 0, 9, 18, 27, 36, 45, 54, 63, 72, 81, 99, 117, 135, 153, 180, 270 |
| Excess REth-heating grid exporting strategies | No excess REth-heating grid exporting;<br>Excess REth-heating grid exporting. |

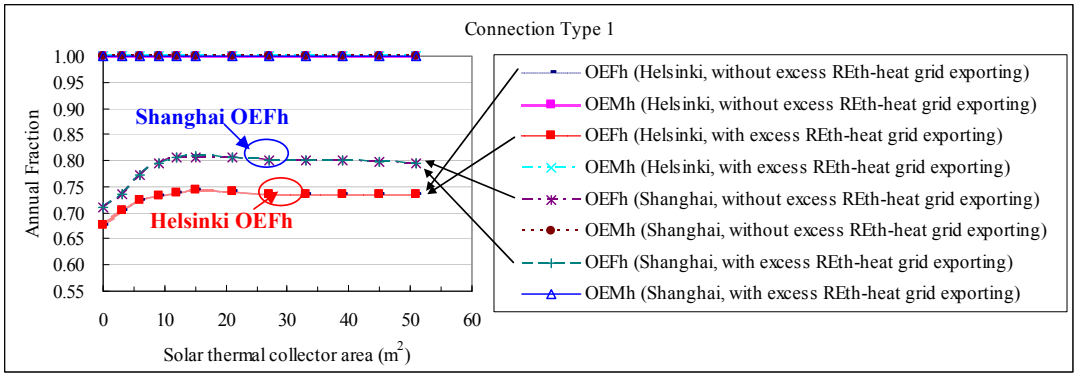


Figure 13. The simulation results of connection Type 1 (all connected in series). Annual heating demands for Helsinki and Shanghai are 35.9 kWh/$m^2$ a and 35.8 kWh/$m^2$ a, respectively. [Original publication III]

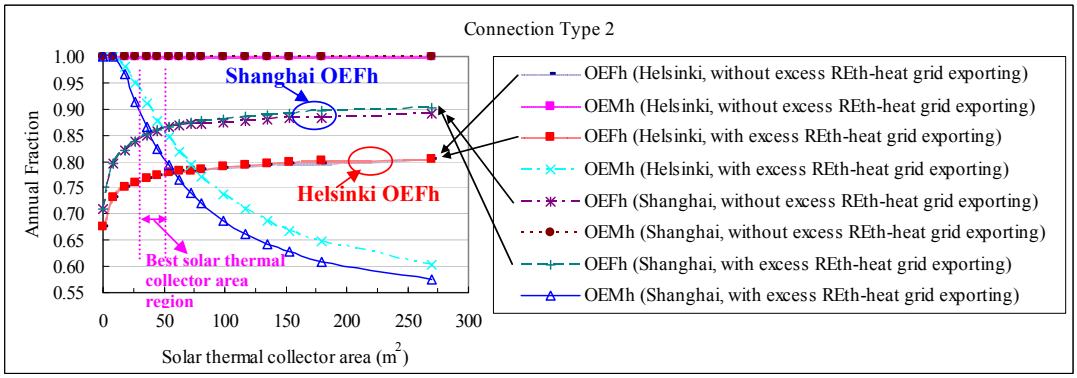


Figure 14. The simulation results of connection Type 2 ("3×n type"). Annual heating demands for Helsinki and Shanghai are 35.9 kWh/$m^2$ a and 35.8 kWh/$m^2$ a, respectively. [Original publication III]

#### 3.2.5.2 PV panel

In this section, a parametric analysis is conducted for the PV system from the aspect of matching with respect to the PV areas, excess REe-thermal recharging strategies and excess REe-grid exporting strategies. The presumption is that the

analysed systems are all equipped with solar thermal collectors in both Helsinki and Shanghai. The parameters of the solar thermal collectors are obtained from the suggestions in Section 3.2.5.1: connection Type 2 ("3×n" type), area of 45 $m^2$, tilt angle of 45° and azimuth angle of due south in both Helsinki and Shanghai. Under the existence of these solar thermal collectors, the annual overall electrical consumptions without excess REe-thermal recharging are around 72.6 kWh/$m^2$ a for Helsinki and 135.7 kWh/$m^2$ a for Shanghai. The PV system follows the technical parameters introduced in Section 3.2.3. The annual generated electricity per $m^2$ at maximum power point (MPP) is 127.8 kWh/$m^2$ a and 151.9 kWh/$m^2$ a (per $m^2$ is based on the total PV area) in Helsinki and Shanghai, respectively. The maximum allowed PV surface areas are 195.8 $m^2$, which is determined based on the considerations of the total roof area (295.5 $m^2$), spaces between PV panels, and the occupations of solar thermal collectors and other equipments. No electrical battery is used in this section. All the options of the studied variables are listed in Table 8. All the combinations of these options are analysed in the simulation.

The annual energy matching results are presented in Figure 15 – Figure 18. Several important points can be concluded: Firstly, the OEMe values are all higher than 0.77, whereas the OEFe values are all lower than 0.4, under the conditions of both Helsinki and Shanghai with respect to all the excess REe treatments. This indicates that most of the electricity produced by PV within the allowable area on the roof is consumed in the office building system. Nevertheless, this PV production is still far from covering all the electrical demands.

Secondly, even without PV panels, the OEFh values are all higher than 0.77 in both Helsinki and Shanghai. This is due to the utilization of on-site solar thermal energy generated by the solar thermal collectors and the on-site renewable heating absorbed from the ground by the ground source heat pump.

Thirdly, as shown in Figure 15 and Figure 16, even without PV panels in Helsinki, the OEFc values are all higher than 0.71. This is due to the on-site renewable cooling produced by the free ground cooling option via the ground heat exchangers. However, in Shanghai, there is no free ground cooling option, and all the on-site cooling is generated by the electrically driven cooling machines (the GSHP in the cooling mode and/or the auxiliary electrically driven chiller). This is the reason why the OEFc curves in Helsinki have almost the same trend as that of the OEFe curves in Shanghai, as shown in Figure 17, with excess REe-electrical grid exporting strategy. When the excess REe-cooling grid exporting strategy is activated in Shanghai, the OEFe curves are a bit higher than the OEFc curves as shown in Figure 18, partly due to the imported off-site cooling from the cooling grid and partly due to the losses of on-site cooling from the cold storage. This difference is the least in Figure 18(c) due to the gain of on-site cooling in the cold storage resulting from

the excess REe-CW recharging strategy.

Fourthly, the excess REe-HW recharging strategy has almost no influence on the OEFe, OEFh, and OEFc. On one hand, as mentioned in the first point, there is a good consistency between the PV production and the electrical demands from the office buildings, making the aggregated excess PV production small. On the other hand, the excess REe mainly occurs in the summer time with abundant solar radiation, whereas the heating demands are only limited to the DHW heating, making the excess REe-HW insignificant.

Fifthly, the excess REe-CW recharging strategy has some influence on the OEFc in Helsinki. It slightly enhances the OEFc by a maximum of 4% when the allowed PV area is within 195.8 $m^2$. However, this effect is negligible in Shanghai. The reason for this is that the cooling demand in Shanghai is much higher than that in Helsinki, making the OEFe lower and OEMe higher in Shanghai than those of Helsinki. This leads to the fact that the aggregated excess REe in Shanghai is not as obvious as that in Helsinki in the summer time, making the excess REe-CW recharging strategy ineffective.

Sixthly, although excess REe-HW and CW recharging strategies have a very small effect in improving OEFe, OEFh and OEFc, they have a noticeable effect in improving certain OEM values. For example, compared between Figure 15(a) and (b), the excess REe-HW recharging strategy helps to enhance the OEMe by a noticeable 12% with a maximum PV area of 195.8 $m^2$ in Helsinki. This means that the excess REe-HW or CW recharging strategy is a solution to handle the excess REe when the exporting stress on the electrical grid is high.

Seventhly, by the excess REe-heating grid or cooling grid exporting strategy, the OEMe can be increased to unity, while the OEMh or OEMc decreases with respect to the increase of the PV area. This indicates that, by altering the excess REe-grid exporting strategies, the stress on the electrical grid can be relieved and the exporting stress can be shifted to the heating or cooling grid. The phenomenon is very significant for the future smart management of hybrid electrical and thermal grid networks.

Table 8. The testing options of excess REe treatments and PV areas [Original publication III].

| | Helsinki | Shanghai |
|---|---|---|
| Excess REe-thermal recharging strategies | No excess REe-thermal recharging;<br>Excess REe-HW recharging<br>Excess REe-CW recharging | No excess REe-thermal recharging;<br>Excess REe-HW recharging<br>Excess REe-CW recharging |
| Excess REe-grid exporting strategies | Excess REe-electrical grid exporting;<br>Excess REe-heating grid exporting. | Excess REe-electrical grid exporting;<br>Excess REe-cooling grid exporting. |
| PV areas ($m^2$) | 0, 17.8, 53.4, 89, 124.6, 160.2, 195.8 | 0, 17.8, 53.4, 89, 124.6, 160.2, 195.8 |

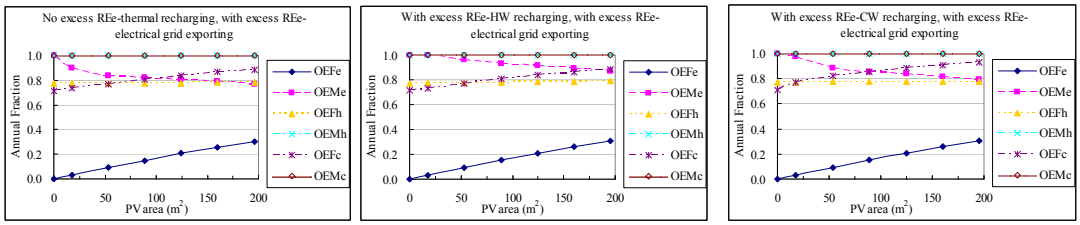


(a) (b) (c)

Figure 15. Influence of PV panel area on the matching indices in Helsinki (excess REe-electrical grid exporting). (a) no excess REe-thermal recharging, (b) with excess REe-HW recharging, (c) with excess REe-CW recharging. [Original publication III]

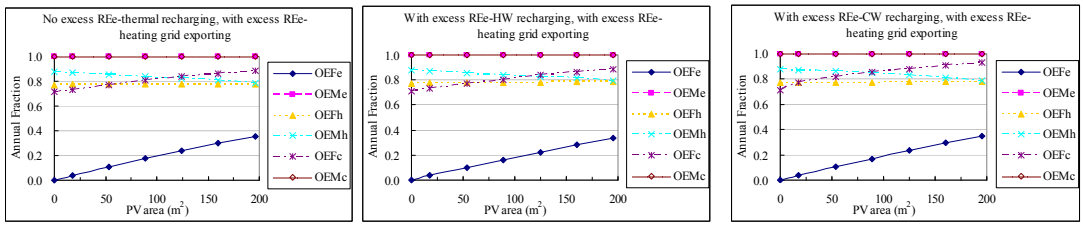


(a) (b) (c)

Figure 16. Influence of PV panel area on the matching indices in Helsinki (excess REe-heating grid exporting). (a) no excess REe-thermal recharging, (b) with excess REe-HW recharging, (c) with excess REe-CW recharging. [Original publication III]

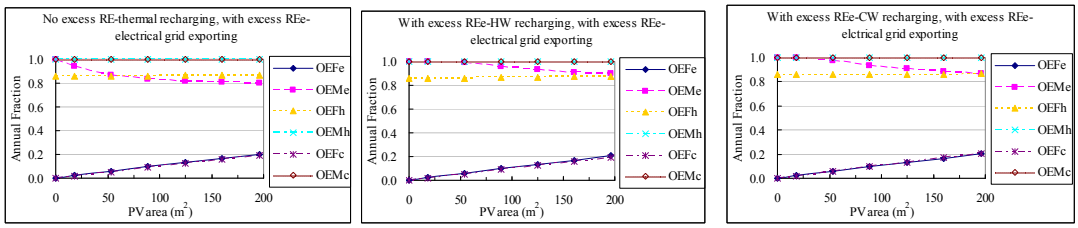


(a) (b) (c)

Figure 17. Influence of PV panel area on the matching indices in Shanghai (excess REe-electrical grid exporting). (a) no excess REe-thermal recharging, (b) with excess REe-HW recharging, (c) with excess REe-CW recharging. [Original publication III]

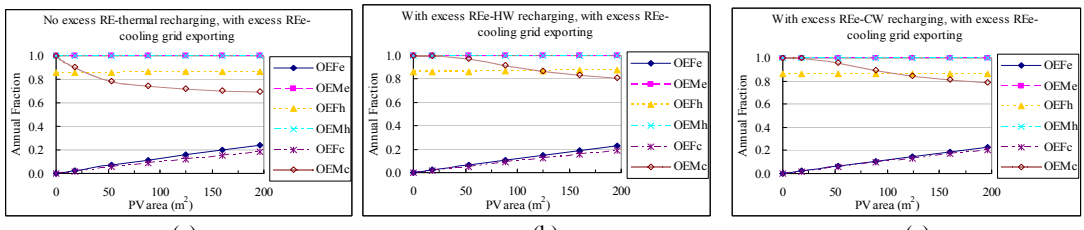


(a) (b) (c)

Figure 18. Influence of PV panel area on the matching indices in Shanghai (excess REe-cooling grid exporting). (a) no excess REe-thermal recharging, (b) with excess REe-HW recharging, (c) with excess REe-CW recharging. [Original publication III]

Figure 19, a continuation to Figure 15(a), is used to illustrate the matching situations of the system when the PV area is larger than the maximum allowed area on the roof in Helsinki. As shown in this figure, the increase ratio of the OEFe and

OEFc curves start to slow down around 500 $m^2$, where the decrease ratio of the OEMe curve also starts to slow down. However, the OEFh curve is not as sensitive as the curves of OEFe and OEFc with respect to the increase of the PV area, because the heating demands are distributed mainly in the winter time when the solar radiation is insufficient.

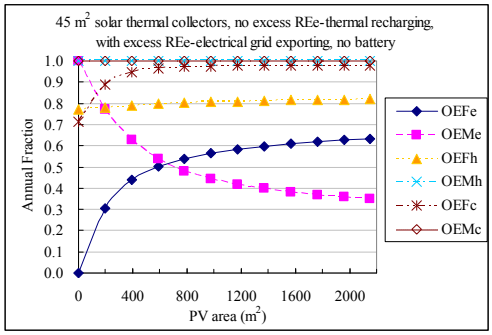


Figure 19. The matching indices when PV area can be larger than the maximum allowable area on the roof in Helsinki. Conditions: no excess REe-thermal recharging, with excess REe-electrical grid exporting, no electrical battery. [Original publication III]

#### 3.2.5.3 Battery

According to the results of Section 3.2.5.2, PV production with the available roof area in both Helsinki and Shanghai is far from covering all the electrical demands, resulting in good OEMe values (OEMe in Helsinki higher than 0.77, OEMe in Shanghai higher than 0.80). With this good OEMe matching capability, Section 3.2.5.2 also shows that excess REe-thermal recharging strategy has a very marginal effect on the improvement of OEFe, OEFh, and OEFc. From an energy point of view, the excess REe-thermal recharging for heat/cold storages mainly contribute to the thermal load, whereas the electrical battery can affect both the electrical and the thermal load. In this section, the parametric analysis of the electrical battery size on the matching capability is conducted. The battery is a lead-acid type battery simulated by Type 47b [43] in TRNSYS. The voltage of the battery system is 48 V, with the upper and lower fractional state of charge at 0.95 and 0.2, respectively. For presenting the influence of the electrical battery, the largest allowable PV area on the roof is used in this section, which is 195.8 $m^2$. The influence of the battery will be less meaningful with a lower PV area, so that a PV area lower than 195.8 $m^2$ is not considered. All the options of the variables are listed in Table 9. All the combinations of the options are taken into account in the simulation. In addition, this section is only focusing on the technical aspect, while the economical aspect is not the focused theme.

Table 9. The testing options of excess REe treatments and battery size [Original publication III].

| | Options |
|---|---|
| Excess REe-thermal recharging strategies | No excess REe-thermal recharging |
| Excess REe-grid exporting strategies | Excess REe-electrical grid exporting |
| Battery size (System voltage of 48 V), Ah | 0, 167, 334, 501, 668, 835, 1002, 1169, 1336, 1503, 1670, 1837, 2004 |

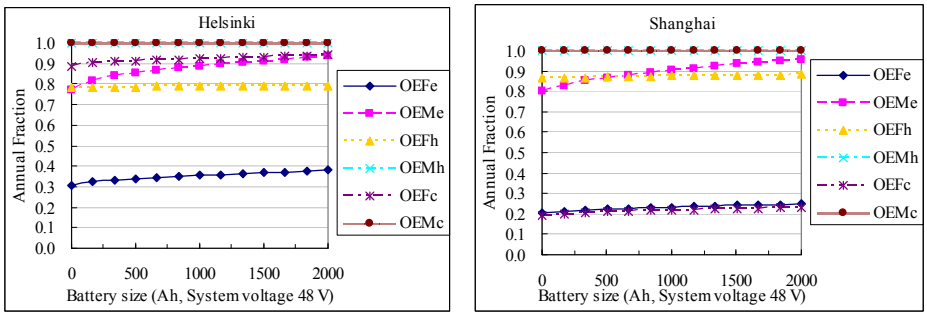


(a) (b)

Figure 20. The simulation results for parametric analysis of electrical battery size (system voltage of 48 V) with 195.8 $m^2$ PV area. All the testing cases are with excess REe-electrical grid exporting strategy, but without excess REe-thermal recharging strategy. (a) for Helsinki and (b) for Shanghai. [Original publication III]

The annual matching results are depicted in Figure 20. Several important points can be noticed. Firstly, as presented in Figure 20(a), with respect to the increase of the battery size from 0-2000 Ah in Helsinki, OEFe increases noticeably by 27% (from 0.30 to 0.38), whereas OEFh and OEFc increase by 1% (from 0.78 to 0.79) and by 6% (from 0.89 to 0.94), respectively. Thus, among the three OEF (OEFe, OEFh, and OEFc), OEFh is the least dependent on the increase of the battery size. This is because in the summer time the electrically driven heating machines are much less frequently used than the electrically driven cooling machines, while the PV production is much higher in the summer time than in the winter time. Moreover, the high level of OEFc in Helsinki is due to the free ground cooling option via the ground heat exchanger.

Secondly, applying the same reason as in Helsinki, the OEFh presents a very slight increase trend with respect to the increase of battery size, as shown in Figure 20(b). Moreover, from 0-2000 Ah, OEFe and OEFc both increase a bit more than 20% in Shanghai. Due to the better OEMe matching between the PV production and electrical demands in Shanghai, the increase trend of OEFe is not as significant as that of Figure 20(a). As already discussed in Section 3.2.5.2, the similar profiles of OEFe and OEFc in Shanghai result from the fact that all the cooling demand is covered by the electrically driven cooling machines, whereas the slightly lower values of OEFc to those of OEFe are due to the on-site renewable cooling losses from the cold storage.

Thirdly, as shown in Figure 20, from 0-2000 Ah, both the OEFe and the OEMe increase by more than 20% in both Helsinki and Shanghai conditions. This indicates that excess on-site PV electricity is effectively stored and utilized by the system. This differs from Figure 15 and Figure 17 in Section 3.2.5.2, where the excess REe-thermal recharging strategy only contributes to the obvious increase of OEMe instead of the OEFe, indicating that a large amount of recharged on-site renewable energy is lost from the thermal storages in the summer time. Therefore, electrical battery is

an effective storage solution for handling the excess REe. However, the cost is a barrier to its utilization. Although this thesis is not focusing on the economic analysis, a rough qualitative estimation can still be made here: according to the current market price, the cost of a 2004 Ah (48 V) lead-acid battery is almost equivalent to 20-30% of the 195.8 $m^2$ PV, while the lifetime of the battery is only around 30-50% of the PV [54], an electrical battery thus not being cost-effective for the purpose.

### 3.2.6 Instantaneous matching analysis

From the above three sections, we can get to some general conclusions:

Firstly, the simulation results in Section 3.2.5.1 show that the connection Type 2 ("3×n type") with the best area range of 36-54 $m^2$ is suitable for the application of solar thermal collectors in both Helsinki and Shanghai. In addition, these solar thermal collectors are all oriented due south with 45° tilt angle for the best annual solar insolations. Secondly, the simulation results of Section 3.2.5.2 show that, with the allowable PV area on the office roof, the PV production is still far from covering all the electrical demands, resulting in good OEMe matching values and poor effects of excess REe-thermal recharging strategies on improving the OEF values (OEFe, OEFh, and OEFc). Thirdly, according to the simulation results of Section 3.2.5.3, the battery proves to be technically effective in storing and utilizing the excess REe from PV systems with large PV areas under the equipment of large battery sizes (up to 2000 Ah, 48 V), but the cost is a barrier to its utilization.

In this section, we show the instantaneous matching situations of the on-site energy systems in both Helsinki and Shanghai. Referring to the conclusions from the above three sections, the on-site renewable energy systems have the following characteristics:

(1) Solar thermal collectors in both Helsinki and Shanghai: connection Type 2 ("3×n type"), an area of 45 $m^2$, 45° tilt angle, due south.

(2) PV systems in both Helsinki and Shanghai: an area of 195.8 $m^2$, 45° tilt angle, due south.

(3) No excess REe-thermal recharging.

(4) Excess REe-electrical grid exporting.

(5) No electrical battery.

August 1st (Wednesday) is selected as the analysed day to show the instantaneous matching situations. Figure 21 and Figure 22 show the simulation results. These instantaneous matching results are obtained by designating $t_1$ and $t_2$ in Equations (5)-(10) equal to the starting and ending of the time-step dt. "dt" is 15 minutes, as mentioned in Section 3.2.1. Figure 21 and Figure 22 illustrate the dynamic instantaneous matching situations between the energy demands and

available on-site renewable energy resources in Helsinki and Shanghai office buildings.

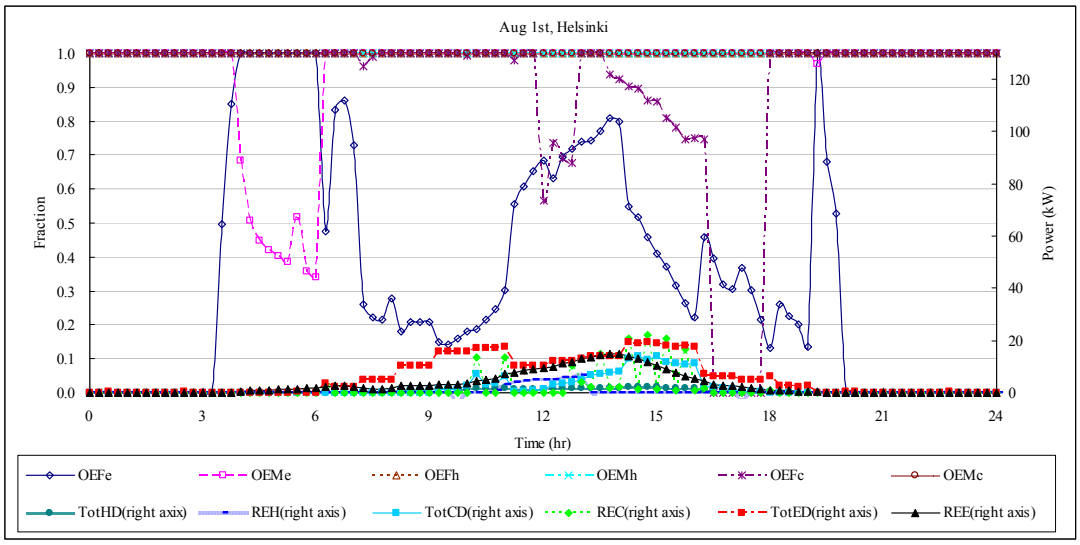


Figure 21. The instantaneous matching indices, power demand, and on-site renewable production for Helsinki on Aug 1st. Abbreviations in the diagram: TotHD: total heating demand power, REH: on-site generated renewable heating power, TotCD: total cooling demand power, REC: on-site generated renewable cooling power, TotED: total electrical demand power, REE: on-site generated renewable electrical power (PV produced power at MPP condition). [Original publication III]

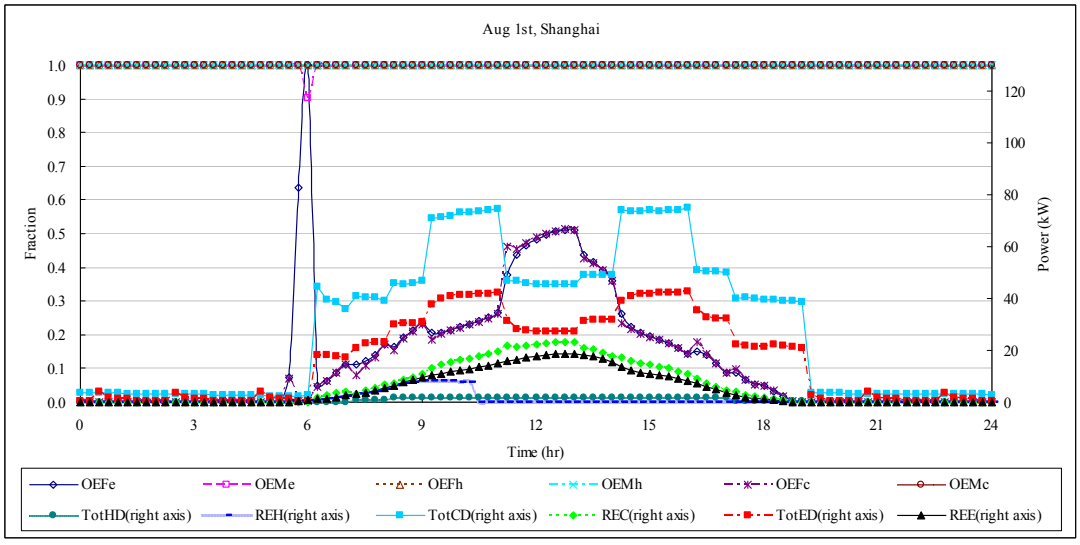


Figure 22. The instantaneous matching indices, power demand, and on-site renewable production for Shanghai on Aug 1st. Abbreviations of labels in the diagram are the same as those stated in Figure 21. [Original publication III]

The instantaneous matching results reflect the matching situations from a micro point of view, but the reflected principles are also in accordance with the annual matching results shown in the above three sections. Firstly, Figure 21 and Figure 22 clearly present the consistency between electrical generation and demand in the daytime in office

buildings. For example, the renewable electrical power is distributed mainly in the daytime between 6:00 and 18:00 in Shanghai, which is also the main distribution period for the total electrical demand power, leading to the corresponding fluctuation of the OEFe curves in the daytime, as shown in Figure 22. Secondly, Figure 21 and Figure 22 clearly show the abundant on-site solar thermal resources for DHW heating in the summer time. For example, in Figure 22 in Shanghai, the total heating demand power (the DHW heating demand power in the summer time) is distributed throughout the daytime, while the renewable heating power (solar thermal heating power in this application) is distributed in the morning to charge the heat storage until it becomes saturated. Meanwhile, the instantaneous OEFh values throughout the day are kept at unity, indicating that 100% of the heating demand is covered by the on-site renewable heating production. Thirdly, the advantages of the free ground cooling can be proved by the comparison of Figure 21 and Figure 22. As shown in Figure 22 for Shanghai office building without free ground cooling, the on-site cooling power is only generated by the on-site part of the electrical power that drives the compressor of the electrically driven cooling machines. Thus, the OEFc curves are with the profiles that are similar to those of the OEFe curves, and the OEFc values are always lower than 53%. However, as shown in Figure 21 for Helsinki, the OEFc curves are mainly distributed above the OEFe curves, due to the free ground cooling in Helsinki.

# 4 Evolvement of extended indices (Original publication IV)

## 4.1 Evolved matching index

From Sections 2 and 3, we can see that the six extended energy matching indices as well as the topology can comprehensively assess the matching situations from all the electrical, heating, and cooling energy forms, while taking the energy conversions, diversified storage types and hybrid grid connections into account. However, these six indices can also bring in some complexity. As the six indices indicate the matching capabilities from six different aspects, the parametric comparison or optimization for a hybrid on-site renewable energy system will be rather sophisticated by all the six assessment criteria. Therefore, it is necessary to define an evolved index based on these six indices, and making this evolved index reflects the overall matching capability where all the six matching aspects are considered. Equation (18) presents a new evolved index — the weighted matching index (WMI). As shown in Equation (18), the WMI is the sum of six terms: each term is calculated by multiplying one of the six extended matching indices by certain weighting factors, $w_i$ , while the sum of these weighting factors is 1.0. These weighting factors show the priorities of preferences on the six extended matching indices. In this way, the WMI essentially reflects the overall matching situation by putting preferences on certain matching aspects. The selection of the weighting factors can be based on various considerations,

such as the environmental impact, political decisions, and economical benefit. This thesis is mainly focused on the development of the concept for the weighted matching index, whereas the selection of weighting factors is not the focused theme in this thesis. However, the selection for the weighting factors will be included in the future work, as presented in Section 7. The WMI is in the range between 0 and 1. A better matching is represented by a higher WMI value, while a WMI equal to unity is the best scenario.

$$\begin{aligned} &\mathrm{WMI}=w_1\mathrm{OEFe}+w_2\mathrm{OEMe}+w_3\mathrm{OEFh}+w_4\mathrm{OEMh}+w_5\mathrm{OEFc}+w_6\mathrm{OEMc}, \\ &\sum_{i=1}^{6} w_i = 1,\ 0 \le w_i \le 1,\ \ 0 \le \mathrm{WMI} \le 1 \end{aligned} \tag{18}$$

A special case for WMI is where the six extended indices have the same weighting factors, i.e. the same preferences. In that situation, $w_i$ is equal to $\frac{1}{6}$, and WMI is essentially the average value of the six extended indices. We refer to the WMI value under this special situation as the "average matching index—AMI". Equation (19) presents the formula for it. When there is no direct instruction on how to select the specific weighting factors, AMI, by giving the same preference to all the six matching aspects, can be used as a very useful tool to show the general comprehensive matching situation.

$$\mathrm{AMI}=\frac{1}{6}\mathrm{OEFe}+\frac{1}{6}\mathrm{OEMe}+\frac{1}{6}\mathrm{OEFh}+\frac{1}{6}\mathrm{OEMh}+\frac{1}{6}\mathrm{OEFc}+\frac{1}{6}\mathrm{OEMc},\ \ 0 \le \mathrm{AMI} \le 1 \tag{19}$$

There is no doubt that by using a single evolved matching index (WMI or AMI), much useful information of the six extended matching indices might be lost. While the evolved index can not solve all of the problems, it should be used as an aiding criterion to show the overall matching situation and the detailed matching aspects should always be investigated by checking the six extended matching indices.

## 4.2 Implementation of evolved matching index

### 4.2.1 Description of the implementation

In this thesis, the evolved index is implemented for the matching assessment of the micro-combined heat and power (mCHP) unit for a single family house. The single family house is a one-storey house with 150 $m^2$ floor area located in Helsinki, Finland. The parameters of envelopes – infiltration, ventilation, and internal gains – are all in accordance with the Finnish Building Regulation D3 2012 [44]. Table 10 lists the annual heating and electrical demands of the studied single family house, while Figure 23 shows the duration curves for the electrical and thermal heat demand powers of the same house. It should be emphasized that the electrical demands presented in Table 10 and Figure 23 exclude the electrical consumptions of the pump (for mCHP) and auxiliary electrical heaters, because the power consumptions of the pump and auxiliary electrical heaters are influenced by the thermal output of the mCHP, which is not constant in the

latter parametric analysis.

Table 10. The heating and electrical demands of the studied single-family house [Original publication IV].

| Annual energy (kWh/m$^2$ a) | | Peak power (kW) | |
|---|---|---|---|
| Heating demands (AHU, space, and DHW heating) | Electrical demands[(a)] (Ventilation fan, lighting, and equipments) | Peak heating demands (AHU, space, and DHW heating) | Peak electrical demands[(a)] (Ventilation fan, lighting, and equipments) |
| 100.3 | 29.9 | 6.0 | 5.6 |

(a) The electrical demands listed in this table exclude the consumptions of the pump (for mCHP) and auxiliary electrical heaters.

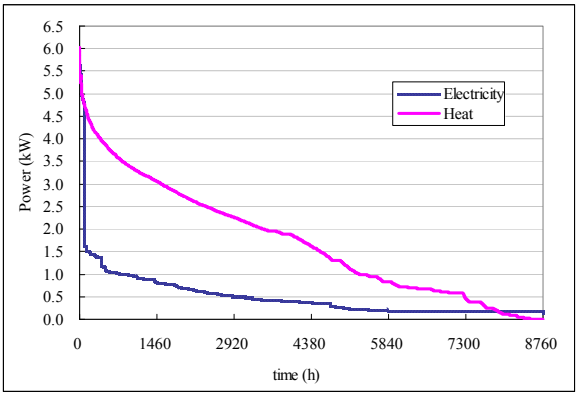


Figure 23. The duration curves for the electrical and thermal heat demand powers of the single-family house. The electrical power in this figure excludes the electrical consumptions of the pump (for mCHP) and auxiliary electrical heaters. [Original publication IV]

Since Section 4 is for showing the methodology by implementing the evolved matching index, the focused parameters of the mCHP products are only limited to the electrical to thermal ratio (ETTR). Furthermore, by reviewing the commercial mCHP products presented in Table 11 and Figure 24, it is found that the most common nominal electrical output power ($G_{elec}$) is 1 kWe, while the ETTR is mainly in the range of 0.05-0.6. Therefore, in the latter parametric analysis, we designate $G_{elec}(t)$ at 1kWe, and the studied range of ETTR from 0.05 to 0.8 with an ETTR step of 0.05, as listed in Table 12. It is assumed that when one mCHP product is in operation, the $G_{elec}$ and ETTR are both kept constant. Furthermore, the size of the hot water storage tank (HWST) and that of the electrical battery are chosen to be values that are suitable to be used and allocated inside the studied single family house: the HWST is a cylindrical vertical storage tank with a volume of 0.3 m$^3$, the electrical battery is a lead-acid battery with a capacity of 100 Ah (48 V). The maximum and minimum limits of the fractional state of the charge (FSOC) of the battery are 0.95 and 0.2, respectively. As the implemented application only refers to two energy forms — electrical and heating energy – the terms OEFc and OEMc can be excluded from the formulae of WMI (Equation (18)) and AMI (Equation (19)), resulting in Equations (20) and (21), respectively:

$$\mathrm{WMI}=w_1\mathrm{OEFe}+w_2\mathrm{OEMe}+w_3\mathrm{OEFh}+w_4\mathrm{OEMh},$$
$$\sum_{i=1}^{4} w_i = 1,\ \ 0 \le w_i \le 1,\ \ \ 0 \le \mathrm{WMI} \le 1 \qquad (20)$$

$$\mathrm{AMI}=\frac{1}{4}\mathrm{OEFe}+\frac{1}{4}\mathrm{OEMe}+\frac{1}{4}\mathrm{OEFh}+\frac{1}{4}\mathrm{OEMh},\ \ 0 \le \mathrm{AMI} \le 1 \qquad (21)$$

In the parametric analysis to follow, the annual matching results of WMI (including AMI) are presented in accordance with Equations (20) and (21) with a time-step of one hour. Due to the limitation of hourly based weather data, internal gains, and occupancy profiles, the time-step used in the simulation is one hour. The author of this thesis always keep in mind that one hour is quite rough for matching analysis because a finer resolution leads to much better accuracy of the matching results. However, during the parametric analysis, all of the simulated cases are kept under the same time-step, so that the comparison of different cases can still be meaningful for the matching analysis of mCHP technologies.

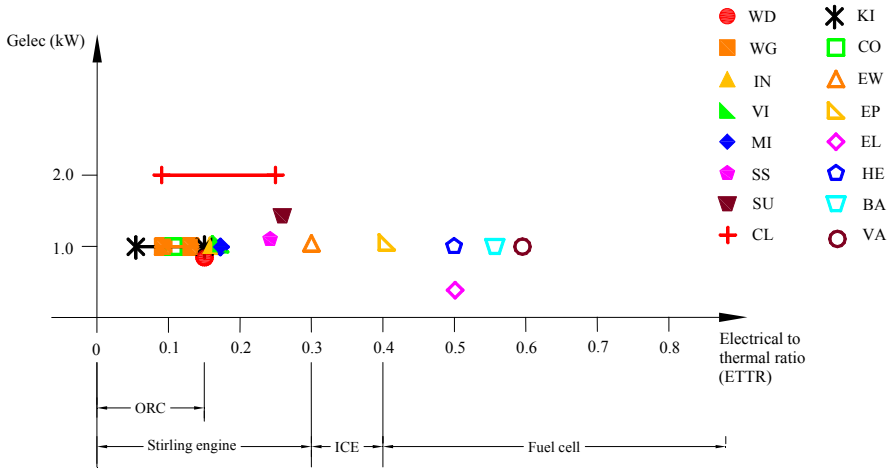


Figure 24. The ETTR ranges with respect to specific mCHP technologies for commercial products on the market. The abbreviations for the product names are indicated in Table 11. [Original publication IV]

Table 11. Reviewed commercial mCHP products [Original publication IV].

| mCHP type | Manufacturer (product) | Nominal electrical power $G_{elec}(t)$, kWe | Nominal thermal heat power $G_{h\_th}(t)$, kWth | Electrical to thermal ratio (ETTR) | Fuel | The abbreviation of products' names | Ref. |
|---|---|---|---|---|---|---|---|
| Stirling engine | Whispergen (Model 12 V diesel fired/24 V diesel fired/ 24 V kerosene fired without grid feed-in option) | 0.8 | 5.5 | 0.15 | Automotive grade diesel | WD | [55] |
| | Whispergen (Model MkV AC Gas Fired with grid feed-in option) | 1.0 | 7.5-12.0 | 0.08-0.13 | Natural gas | WG | [55] |
| | Infinia | 1.0 | 6.4 | 0.16 | Solar heat, biogas, and natural gas | IN | [56] |
| | Viessmann (Vitotwin 300-W) | 1.0 | 6.0 | 0.17 | Natural gas | VI | [57] |
| | Microgen | 1.0 | 6.0 | 0.17 | Existing device is based on natural gas, but Microgen is investing in other fuel sources, including biomass, solar heat, and waste heat. | MI | [58] |
| | Stirling Systems Ltd. | 1.2 | 5.0 | 0.24 | Hydrocarbon: fossil fuel, biomass | SS | [59] |
| | Sunmachine | 1.4 | 5.4 | 0.26 | Pellets (wood) | SU | [60] |
| | Cleanergy | 2.0 (Max. 9.0) | 8.0-25.0 | 0.08-0.25 | Bio-gas, natural gas | CL | [61] |
| Organic Rankine Cycle (ORC) | Energetix Genlec Ltd. (Kingston) | 1.0 | 6.8-18.0 | 0.06-0.15 | Natural gas, liquefied petroleum gas and other fuel sources that can provide an adequate heat flow and temperature | KI | [62] |
| | Cogen Microsystems | 1.0 | 8.8 | 0.11 | Solar heat | CO | [63] |
| Internal combustion engine (ICE) | Honda (Ecowill) | 1.0 | 3.3 | 0.3 | Natural gas, liquid propane | EW | [64] |
| | Honda and Vaillant (ecoPOWER 1.0) | 1.0 | 2.5 | 0.4 | Natural gas, liquid propane | EP | [64] |
| Fuel cell | Elcore (Elcore 2400) | 0.3 | 0.6 | 0.5 | Natural gas | EL | [65] |
| | Hexis (Galileo 1000 N) | 1.0 | 2.0 | 0.5 | Natural gas | HE | [66] |
| | BAXI INNOTECH GmbH (GAMMA 1.0) | 1.0 | 1.8 | 0.56 | Natural gas | BA | [67] |
| | Vaillant | 1.0 | 1.7 | 0.59 | Natural gas | VA | [68] |

Table 12. The options for the $G_{elec}$ and ETTR.

| | Options |
|---|---|
| Electrical output (kWe) | 1.0 |
| Electrical to thermal ratio | 0.05 to 0.80 with 0.05 step |

Normally, mCHP products have the maximum allowed temperatures of the heat transfer fluid (HTF) supplied from and returning to the mCHP; thus, prior to the introduction of the control principles, the assumption is made that the maximum allowed temperatures of the heat transfer fluid (HTF) supplied from and returning to the mCHP are 65 and 55

ºC, respectively. These selections are based on the consideration that the set point of the DHW is 55 ºC. There are two control strategies used for the mCHP. Figure 25 presents a brief schematic for the control principle of the thermal tracking strategy, while Figure 26 presents a brief schematic for the control strategy of the electrical tracking strategy. The control principle for the thermal tracking strategy is as follows. As shown in Figure 25, the operation of the mCHP is controlled by the tank temperature. When the bottom tank temperature $T_1$ is higher than 55 ºC, both the mCHP and the pump should be turned off to prevent the HTF returning back to the mCHP from being higher than 55 ºC. When the bottom tank temperature $T_1$ is lower than 55 ºC, both the pump and the mCHP should be turned on. For each analysed mCHP product, a specific mass flow rate through the pump is selected so that the HTF temperature difference before and after the mCHP product ($T_2$ and $T_3$) would be equal to 10 ºC. In this way, the supply temperature from the mCHP will never exceed 65 ºC. The HTFs for the DHW, AHU and space heating purposes flow through the HWST to extract the heating before passing through the auxiliary heating device by the electrical heater. The electrical power generated from the mCHP is first sent to meet the electrical demands. On one hand, if the generated electrical power is higher than the electrical demands, the surplus will be sent to charge the battery; thereafter, any surplus generated electrical power will be fed into the electrical grid. On the other hand, if the generated electrical power is lower than the electrical demands, the battery will be discharged to meet the shortage; thereafter, any remaining shortage will be covered by the electrical power imported from the electrical grid.

The control principle for the electrical tracking strategy is as follows. As shown in Figure 26, the operation of the mCHP is controlled by the fractional state of charge (FSOC) of the electrical battery. On one hand, when the FSOC is higher than 0.95, both the pump and the mCHP should be turned off. On the other hand, when the FSOC is lower than 0.3, both the pump and the mCHP should be turned on. The reason why the start-up FSOC is not the lowest limit (FSOC=0.2) is to reduce the number of times the battery is at its deepest FSOC when the electricity has to be merely imported from the electrical grid to cover the shortage. Since the operation of the mCHP is not controlled by the HWST temperature, the bottom tank temperature $T_1$ might exceed 55 ºC. In order to prevent the temperature of the HTF returning back to the mCHP from being higher than 55 ºC, a heat exchanger is equipped before the inlet of the mCHP to process the heat exportation to the local heating grid. An assumption is made that when $T_1$ is higher than 55 ºC the HTF will experience the heating grid feed-in process, and the returning HTF temperature after the feed-in process will be kept at 55 ºC. Since the local heating grid exists, the auxiliary heating device is by the heating grid instead of the electrical heater. The treatment of the generated electrical power is the same as what has been described for the thermal tracking strategy.

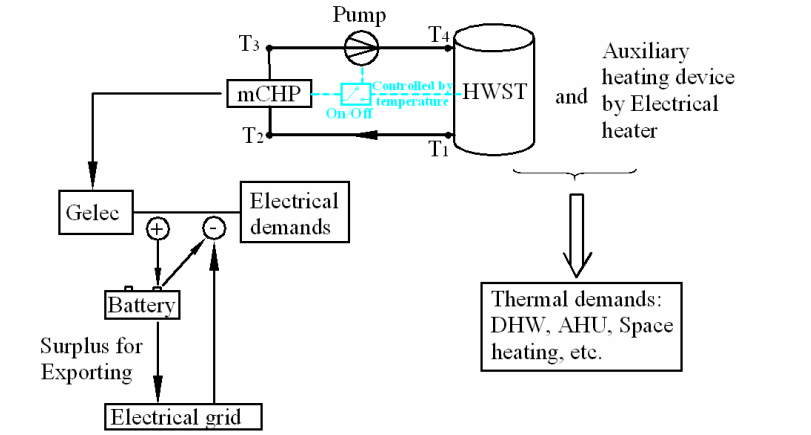


Figure 25. The brief schematic of the control principle for the thermal tracking strategy [Original publication IV].

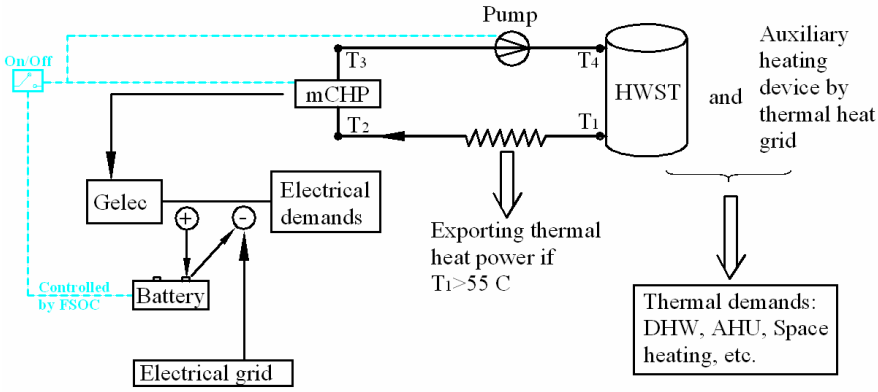


Figure 26. The brief schematic of the control principle for the electrical tracking strategy [Original publication IV].

### 4.2.2 WMI for the thermal tracking strategy

It should be mentioned that this thesis is not focused on the selection of weighting factors but uses simple assumptions to reflect the impact of weighting factors on the WMI values. Therefore, we choose four simple examples for which four groups of weighting factors are designated, as listed in Table 13. The underlying principle in Example A is that electrical matching is more important than thermal heat matching, while in Example B it is the other way round. Thus, the weighting factors $w_1$ - $w_4$ in Example A have the values 0.375, 0.375, 0.125, and 0.125, respectively, while the corresponding values in Example B are 0.125, 0.125, 0.375, and 0.375. Moreover, the underlying principle in Example C is that covering the local demand by on-site generation (i.e. OEF) is more important than utilizing the on-site generation by local demand (i.e. OEM), whereas in Example D it is the other way round. Thus, $w_1$ - $w_4$ in Example C have the

values 0.375, 0.125, 0.375, and 0.125, respectively, while the corresponding values in Example D are 0.125, 0.375, 0.125, and 0.375. In practice, Example A can happen to a situation where the house owner pays more attention to the electrical matching than heat matching, for example because the electrical grid tariff is much more expensive than the district heating tariff; Example B can happen to a situation where the house owner pays more attention to the heat matching than electrical matching, for example because the district heating tariff is much more expensive than the electrical grid tariff; Example C can happen to a situation where the house owner tries to meet the low-energy or zero-energy balance of the house, or to a situation where the feed-in tariff to the (electrical and heat) grid is much more expensive than the import tariff; Example D can happen to a situation where the feed-in tariff to the (electrical and heat) grid is zero or much less than the import tariff and the house owner tries to utilise the on-site generation for the local demand to the largest extent.

Table 13. Four examples of the weighting factors [Original publication IV].

| Example | Underlying Principle | $w_1$ (a) | $w_2$ (a) | $w_3$ (a) | $w_4$ (a) |
|---|---|---|---|---|---|
| A | Electrical matching is more important than thermal heat matching | 0.375 | 0.375 | 0.125 | 0.125 |
| B | Thermal heat matching is more important than electrical matching | 0.125 | 0.125 | 0.375 | 0.375 |
| C | Covering the local demand by on-site generation is more important than utilizing the on-site generation by local demand | 0.375 | 0.125 | 0.375 | 0.125 |
| D | Utilizing the on-site generation by the local demand is more important than covering the local demand by on-site generation | 0.125 | 0.375 | 0.125 | 0.375 |

(a) According to Equation (20), $w_1$, $w_2$, $w_3$, and $w_4$ are the weighting factors for OEFe, OEMe, OEFh, and OEMh, respectively.

Figure 27 presents the simulation results of the annual WMI values of the four examples with respect to certain ETTR while Figure 28 presents the simulation results of the annual extended indices' values with respect to certain ETTR. Also the AMI curves are illustrated in Figure 27 and Figure 28 for comparison purposes. Due to the thermal tracking strategy, the thermal matching is better than the electrical matching, leading to that the WMI_A curve is below the AMI curve whereas the WMI_B curve is above the AMI curve. The difference between the WMI_A curve and WMI_C curve is mainly seen at the ETTR range from 0.4 to 0.8. This is due to the thermal tracking strategy: with the increase of the ETTR, the on-site generated heating power $G_{h\_th}(t)$ continuously decreases, and the heating demand will rely more on the auxiliary electrical heaters; this leads to the decrease of OEFh, especially when the ETTR is higher than 0.4, as shown in Figure 28. The weighting factors $w_1$ and $w_4$ are respectively the same in Example A and Example C, while OEMe is always with a high value (above 0.86, as shown in Figure 28) with respect to all of the ETTR ranges due to the electrical battery. Therefore, the difference between the WMI curves in case of Examples A and C will be more sensitive to the fluctuation of OEFh than to other extended indices. In this way, when $w_3$ (0.375) of Example C is greater than $w_3$ (0.125) of Example A, the decrease of OEFh results in a more obvious drop of WMI_C than in WMI_A. The difference between the WMI_B and WMI_D curves can be explained with a similar manner.

Moreover, as shown in Figure 27, all the WMI curves, including the AMI curve, peak at around the ETTR of 0.3. According to the illustration for the review of commercial products presented in Figure 24, this ETTR around 0.3 is in the range of the Stirling engine and internal combustion engine (ICE). In addition, Figure 27 also shows the commercial products whose ETTR values are close to the peak of the WMI and AMI curves. The product of "EW: Honda (Ecowill)" points to (or close to) the peaks of all WMI and AMI curves, while the product of "SS: Stirling Systems Ltd." points to (or close to) the peaks of WMI_B and WMI_D curves.

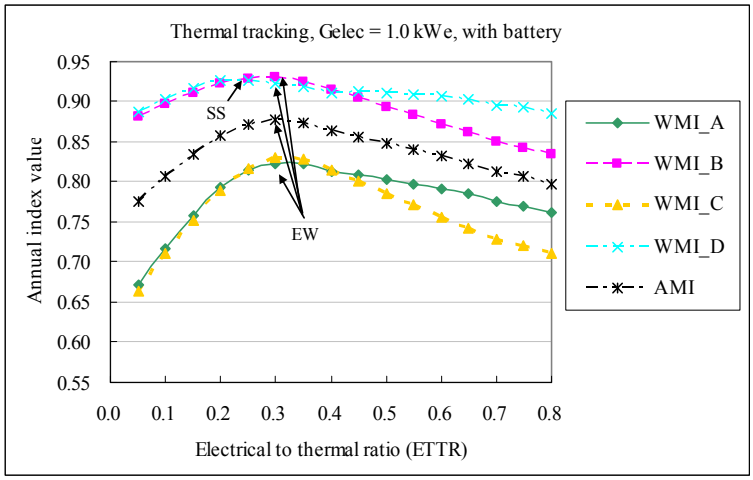


Figure 27. The impact of the weighting factor on the WMI curve under the condition of thermal tracking with battery, with $G_{elec}$ of 1.0 kWe. The abbreviations for the product names (SS, EW) can be checked in Table 11. [Original publication IV]

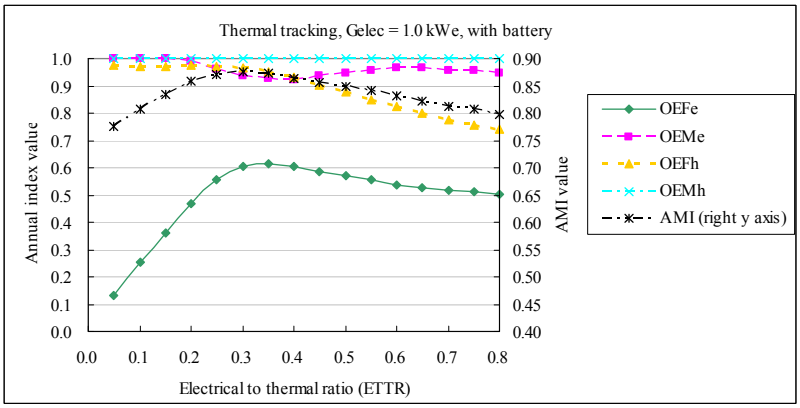


Figure 28. The detailed four matching indices and AMI for thermal tracking with battery under $G_{elec}$ of 1.0 kWe [Original publication IV].

### 4.2.3 WMI for the electrical tracking strategy

Figure 29 presents the simulation results of the annual WMI values of the mCHP with respect to the ETTR under electrical tracking strategy, while Figure 30 presents the simulation results of the annual extended indices' values of the mCHP under the electrical tracking strategy. In addition, the AMI curves are illustrated in Figure 29 and Figure 30 for comparison purposes. The four examples still follow the assumptions listed in Table 13. Due to the electrical tracking strategy, the electrical matching is better than the thermal heat matching, leading to the fact that the WMI_A curve is above the AMI curve whereas the WMI_B curve is below the AMI curve. The WMI_A and WMI_C curves have similar profiles at the ETTR range of 0.05 and 0.2; however, as the ETTR increases from 0.2, the WMI_C curve continuously decreases whereas WMI_A is relatively stable. This can be explained as follows. Under the electrical tracking strategy, with the increase of ETTR, the generated thermal heat power ($G_{h\_th}(t)$) by the mCHP continuously decreases, and heating demand is more dependent on the auxiliary heating device, i.e. the heating grid. Therefore, as ETTR increases from 0.05 to 0.80, the OEMh continuously increases, while the OEFh continuously decreases; meanwhile, OEFe and OEMe both stabilise above 0.9, as shown in Figure 30. Considering the weighting factors of Examples A and C listed in Table 13, the difference between the WMI_A and WMI_C curves is more sensitive to the fluctuation of OEFh than to other extended indices. With higher $w_3$ (0.375) of Example C than that (0.125) of Example A, the WMI_C curve significantly decreases when the ETTR increases from 0.2 to 0.8. The difference between the WMI_B and WMI_D curves can be explained in a similar manner.

Moreover, as shown in Figure 29, the curves of WMI_A, WMI_B, and AMI peak around the ETTR of 0.25-0.3 (Stirling engine, ICE), while the curves of WMI_C and WMI_D peak around 0.2 (Stirling engine) and 0.8 (fuel cell), respectively. Regarding the commercial products reviewed in Table 11, "SS: Stirling Systems Ltd." and "EW: Honda (Ecowill)" point to (or close to) the peaks of WMI_A, WMI_B, and AMI curves, while the products of "VI: Viessmann (Vitotwin 300-W)" and "MI: Microgen" point to (or close to) the peak of WMI_C curve. Among the reviewed commercial products in Table 11, "VA: Vaillant" is the product with the highest WMI value referring to the WMI_D curve. Therefore, it is very important to notice that by selecting different weighting factors, the overall matching situations as well as the peak matching points can vary, which might influence the final decision.

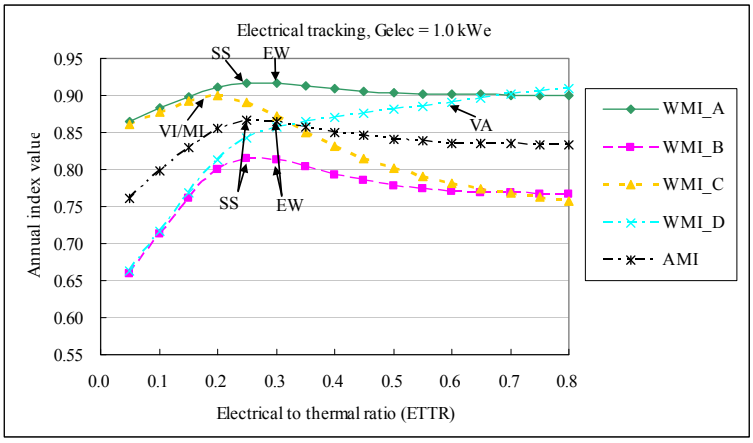


Figure 29. The impact of the weighting factors on the WMI values. The abbreviations for the product names (VI, MI, SS, EW, VA) can be checked in Table 11. [Original publication IV]

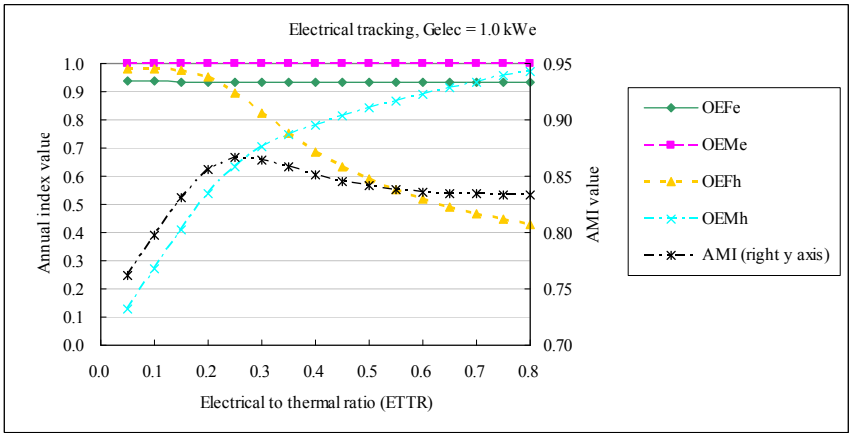


Figure 30. The detailed four matching indices and AMI for the electrical tracking strategy under $G_{elec}$ of 1.0 kWe [Original publication IV].

# 5 Summary of the new contributions

This thesis is based on the new contributions of the journal papers conducted during the author's doctoral study period. The new contributions of original publication I are represented by two aspects. The first aspect is to show the importance of the analysis for on-site matching, especially for the buildings equipped with significantly enhanced on-site renewable energy systems. The second aspect is to provide a solution, i.e. the excess REe-DHW recharging strategy, for effectively reducing the on-site electrical mismatch. Based on the study in the original publication I and corresponding reviews, there is an urgent need for proposing a methodology that can comprehensively handle the on-site energy matching analysis considering all the energy forms, diversified energy conversions, various storage systems and hybrid grid

network connections. The new contribution of original publication II exclusively meets this need by proposing six extended matching indices and one generalised topology. The implementation of these extended matching indices and topology is thereafter carried out in original publication III for the design and analysis of two advanced office buildings with enhanced hybrid on-site renewable energy systems and bi-directionally connected hybrid grid connections. Moreover, original publication III lists the diversified excess REe and REth treatments, which are options that might significantly influence specific matching aspects in the future hybrid energy networks; thus, in original publication III, those relevant specific matching aspects are all investigated through the parametric analysis with the aid of the extended indices and the topology. Finally, the new contribution of original publication IV is proposing the evolved matching indices of WMI and AMI based on the extended indices. This new contribution is very important, because the usage of the evolved matching indices together with the extended indices can analyse the matching situation from both the overall viewpoint and the detailed specific viewpoints.

# 6 Conclusions

Under the background that all new buildings in EU should be nearly zero-energy buildings (nZEB) from the year 2021, the energy and building industries are progressing towards the direction of decreased local building energy demands and enhanced on-site renewable energy systems. This, on one hand, leads to continuously decreased annual primary energy consumption/equivalent $CO_2$ emissions, whereas on the other hand, it brings in the matching problem between the on-site generation and local building demands. Considering the fact that the renewable energy fraction in the hybrid energy grid networks is not likely to reach 100% by the year of 2021, the mismatch is an inevitable side-effect of low-energy or even net-zero energy buildings. Therefore, suitable criteria should be established to quantitatively assess the matching situations.

There are two basic matching indices which are commonly used in the scientific community: one is on-site energy fraction (OEF), indicating the proportion of the demand covered by the on-site production; the other one is on-site energy matching (OEM), indicating the proportion of the on-site generation consumed in the building and system rather than being exported or dumped. However, the applicability of these two basic matching indices is significantly limited, because with the fast development of the energy technology, the matching assessment deals with all energy forms, various energy conversions, diversified storage systems and future bi-directionally connected hybrid grid networks. In order to handle these challenges, this thesis proposes six extended matching indices based on the extension of the two

basic matching indices. Three of the extended indices — OEFe, OEFh, and OEFc — are based on the extension of the OEF while the other three — OEMe, OEMh, and OEMc — are based on the extension of the OEM; the postfixes of "e", "h", and "c" represent the electrical, heating, and cooling aspects, respectively. Furthermore, one generalised topology (Figure 4) is proposed for the understanding and formulation of the six extended matching indices.

In order to show the applicability of these extended indices, a comprehensive matching analysis is conducted for the components of on-site hybrid renewable energy systems of two office buildings: one in Helsinki with high-latitude heating-dominant climate conditions and one in Shanghai with subtropical cooling-dominant climate conditions. For the office buildings in both Helsinki and Shanghai, the on-site hybrid energy systems are solar (PV and solar thermal) assisted ground source heat pumps that are bi-directionally connected with hybrid energy grid networks. Due to the various storages, energy conversion machines and hybrid grid connections, the excess renewable electrical (REe) or renewable thermal (REth) treatments are diversified. For the office applications, there are six excess REe treatments, i.e. three excess REe-thermal recharging strategies and three excess REe-grid exporting strategies. In addition, one excess REth treatment is also taken into account. With the aid of the six extended indices, a parametric analysis is conducted from the aspect of matching for the solar thermal collector connection type and area, PV panel area and the electrical battery size. The annual and instantaneous matching results both show the advantages of the solar thermal collectors connected in a parallel fashion for meeting the heating demands, the consistency between the solar resources and office (electrical and thermal) demands in the daytime, and the effective influence of electrical battery in improving the electrical matching aspects. The implementation processes as a whole prove the applicability of the methodology in aiding the analysis and design for increasingly complicated on-site hybrid renewable energy systems.

The six extended matching indices represent six aspects of the matching capability of the assessed on-site energy systems. This makes the matching assessment very comprehensive and thorough for the energy systems, but it also brings in complexity for the comparison, optimization or decision making processes. Therefore, this thesis defines one further evolved index, i.e. weighted matching index (WMI), based on the six extended matching indices. This WMI is calculated by the sum of six terms, each term being a multiplication of one extended index by a certain weighting factor. The weighting factor represents the preference for a certain aspect of the matching, and the sum of the weighting factors is one. Moreover, there is a special situation for WMI when all the extended indices have the same preference and all the matching indices are with the same value. This leads to an average matching index (AMI), which is essentially the average value of the six extended matching indices. In this way, we can use one index instead of six indices to investigate the overall matching capability for on-site energy systems. This thesis is not focusing on the selection of

weighting factors, because the process of selection can depend on many factors, such as political decisions, environmental influence, and economical considerations. In order to implement WMI (or AMI), this thesis implements WMI (or AMI) for the matching analysis of the mCHP units for meeting the electrical and thermal heat demands of a single family house. The results show the influence of weighting factors on the final comprehensive matching results (annual WMI or AMI results). The selected commercial products, referring to the best annual WMI or AMI value, might be altered by designating different weighting factors. Moreover, by mutual investigation of the evolved index (WMI or AMI) and the extended matching indices (OEFe, OEFh, OEFh, OEMe, OEMh, and OEMc), both the overall matching capability and the detailed specific matching aspects can be effectively presented.

# 7 Future work

Firstly, it is important to investigate the role of nearly zero energy buildings or net zero energy buildings in future bi-directionally connected hybrid energy grid networks. This can be done with the methodology developed in this thesis. The focused research points can include management of on-site energy generation systems, smart control for energy conversion and storage processes, responsive control for demand side management, and dynamic interaction with hybrid energy grid networks.

Secondly, the impact of the time-resolution on the matching capability should also be conducted in the future work. As mentioned in Section 2, both the OEF and OEM would possibly be overestimated by using the coarser resolution. By the methodology developed in this thesis, it will be interesting to evaluate the impact of the specific time resolutions on the matching capability for various on-site energy systems, such as PV and wind turbine.

Thirdly, the matching analysis can be extended from a single low/zero-energy building to a low/zero-energy community. The differences in and interactions of the matching characteristics of a single building and a community should be investigated. This can involve the following research questions: how can on-site energy generation be shared between the loads of the buildings within a community; how can energy conversion and energy storages be controlled within a community; what is the function of the local hybrid energy grid networks which are internally connected inside a community; what is the role of the community in the future large scale urban hybrid energy grid networks which are externally connected to that community.

Fourthly, as mentioned in Section 4, the selection of weighting factors for the weighted matching index (WMI) can be based on various considerations, such as the environmental impact, political decisions, and economical benefit. Future work will investigate the methodology to correlate these considerations with the formulation of the weighting factors. The aim is to make the WMI reflect both the matching situations and the information for certain considerations.

Fifthly, the extended matching indices and the evolved indices are very promising criteria for single or multi-objective optimization problems for the design of high performance buildings with enhanced on-site energy systems. An interesting topic is to compare the difference between a single objective optimization result where WMI is considered as the criterion and a result of the multi-objective optimization where several extended matching indices are considered as the criteria. Moreover, by considering the criteria, such as primary energy consumption and cost, together with the matching indices, the optimization processes can be made more extensive and comprehensive.

# 8 References


[1] S.B. Sadineni, S. Madala, R.F. Boehm, Passive building energy savings: A review of building envelope components, Renewable and Sustainable Energy Reviews 15 (2011) 3617-3631.

[2] S. Cao, State of the art thermal energy storage solutions for high performance buildings. MSc thesis. Jyväskylä, Finland: University of Jyväskylä / The Research Centre on Zero Emission Buildings (ZEB), Norwegian University of Science and Technology (NTNU) / SINTEF Building and Infrastructure, 2010. [Online]. Available: Jyväskylä University Digital Archive (JYX).

[3] S.S. Moody, D.J. Sailor, Development and application of a building energy performance metric for green roof systems, Energy and Buildings 60 (2013) 262-269.

[4] T. Gil-Lopez, C. Gimenez-Molina, Influence of double glazing with a circulating water chamber on the thermal energy savings in buildings, Energy and Buildings 56 (2013) 56-65.

[5] A. Mardiana-Idayu, S.B. Riffat, Review on heat recovery technologies for building applications, Renewable and Sustainable Energy Reviews 16 (2012) 1241-1255.

[6] A.D. Rosa, J.E. Christensen, Low-energy district heating in energy-efficient building areas, Energy 36 (2011) 6890-6899.

[7] A. McNabola, K. Shields, Efficient drain water heat recovery in horizontal domestic shower drains, Energy and Buildings 59 (2013) 44-49.

[8] X. Zhang, X. Zhao, S. Smith, J. Xu, X. Yu, Review of R&D progress and practical application of the solar photovoltaic/thermal (PV/T) technologies, Renewable and Sustainable Energy Reviews 16 (2012) 599-617.

[9] F. Cucchiella, I. D'Adamo, M. Gastaldi, S.C.L. Koh, Renewable energy options for buildings: Performance evaluations of integrated photovoltaic systems, Energy and Buildings 55 (2012) 208-217.

[10] S.L. Walker, Building mounted wind turbines and their suitability for the urban scale—A review of methods of estimating urban wind resource, Energy and Buildings 43 (2011) 1852-1862.

[11] H. Ibrahima, A. Ilincaa, J. Perronb, Energy storage systems-Characteristics and comparisons, Renewable and Sustainable Energy Reviews 12 (2008) 1221-1250.

[12] Electricity Storage Association, "Technology Comparison," Electricity Storage Association, 2011. [Online]. Available: http://www.electricitystorage.org/technology/storage_technologies/technology_comparison.

[13] A. Capozza, M.D. Carli, A. Zarrella, Design of borehole heat exchangers for ground-source heat pumps: A literature review, methodology comparison and analysis on the penalty temperature, Energy and Buildings 55 (2012) 369-379.

[14] "DIRECTIVE 2010/31/EU of the European Parliament and of the Council of 19 May 2010 on the energy performance of buildings," The European Parliament and the Council of the European Union, 19 May 2010.

[15] A.J. Marszal, P. Heiselberg, J.S. Bourrelle, E. Musall, K. Voss, I. Sartori, A. Napolitano, Zero Energy Building – A review of definitions and calculation methodologies, Energy and Buildings 43 (2011) 971-979.

[16] S. Attia, M. Hamdy, W. O'Brien, S. Carlucci, Assessing gaps and needs for integrating building performance optimization tools in net zero energy buildings design, Energy and Buildings 60 (2013) 110-124.

[17] S. Conti, S. Raiti, Probalistic load flow using Monte Carlo techniques for distribution networks with photovoltaic generators, Solar Energy 81 (2007) 1473-1481.
[18] S. Cobben (Continuon), B. Gaiddon (Hespul), H. Laukamp (Fraunhofer ISE), "WP4 – Delivarable 4.3: Impact of photovoltaic generation on power quality in urban areas with high PV population – results from monitoring campaigns," PV UPSCALE Urban Scale Photovoltaic Systems, 14 July 2008. [Online]. Available: http://www.pvupscale.org/.
[19] S.J. Corner, Distributed Dispatching for Embedded Generation. PhD [Dissertation]. Glasgow: University of Strathclyde, 2003. [Online]. Available: http://www.esru.strath.ac.uk.
[20] M. Bollen, F. Hassan, Integration of distributed generation in the power system, John Wiley & Sons, 2011.
[21] M. Braun, T. Stetz, R. Bründlinger, C. Mayr, K. Ogimoto, H. Hatta, et al., Is the distribution grid ready to accept large-scale photovoltaic deployment? State of the art, progress, and future prospects. Progress in Photovoltaics 20 (2012) 681-97.
[22] IEA Photovoltaic Power System Programme, "National Survey Reports," iea-pvps.org – National Reports, 2014. [Online]. Available: http://www.iea-pvps.org/index.php?id=93.
[23] EPIA Policy and Communications Working Group, "Self Consumption of PV Electricity, Position Paper," European Photovoltaic Industry Association, Renewable Energy House, July 2013. [Online]. Available: http://www.epia.org/fileadmin/user_upload/Position_Papers/Self_and_direct_consumption_-_position_paper_-_final_version.pdf.
[24] F. Born, Aiding Renewable Energy Integration through Complementary Demand-Supply Matching. PhD [Dissertation]. Glasgow: University of Strathclyde, 2001. [Online]. Available: http://www.esru.strath.ac.uk.
[25] P. Mathew, V. Hartkopf, A. Mahdavi, Towards the Building as a Power Plant: Computational Analysis of Building Energy Self-Sustenance. Proceedings of Building Simulation 1999, International Building Performance Simulation Association (IBPSA).
[26] J. Widén, E. Wäckelgård, P. Lund, Options for improving the load matching capability of distributed photovoltaics: Methodology and application to high-latitude data, Solar Energy 83(2009) 1953-1966.
[27] K. Voss, I. Sartori, A. Napolitano, S. Geier, H. Goncalves, M. Hall, P. Perselberg, J. Widen, J.A. Candanedo, E. Musall, B. Karlsson, P. Torcellini, Load matching and Grid Interaction of Net Zero Energy Buildings. EuroSun 2010, Graz Austria, September 29th-October 1st.
[28] J. Salom, J. Widen, J. Candanedo, I. Sartori, K. Voss, and A. Marszal, Understanding net zero energy buildings: evaluation of load matching and grid interaction indicators. Proceedings of Building Simulation 2011: 12th Conference of International Building Performance Simulation Association (IBPSA), Sydney, November14th-16th.
[29] B. Verbruggen, R.D. Coninck, R. Baetens, D. Saelens, L. Helsen, J. Driesen, Grid Impact Indicators for Active Building Simulation. IEEE PES Conference on Innovative Smart Grid Technologies 2011, Anaheim, California, US, January 17-19.
[30] G. Mulder, F.D. Ridder, D. Six, Electricity storage for grid-connected household dwellings with PV panels, Solar Energy 84 (2010) 1284-1293.
[31] J.D. Mondol, Y.G. Yohanis, B. Norton, Optimising the economic viability of grid-connected photovoltaic systems. Applied Energy 86 (2009) 985-999.
[32] L. Wissing, Forschungszentrum Jülich GmbH, "National Survey Report of PV Power Applications in Germany 2011," National Survey Reports for Germany, IEA Photovoltaic Power System Programme, July 2012. [Online]. Available: http://www.iea-pvps.org/index.php?id=93&eID=dam_frontend_push&docID=1234.
[33] M. Lang, U. Mutschler, "German Feed-in Tarrifs 2012," German Energy Blog, 2012. [Online]. Available: http://www.germanenergyblog.de/?page_id=8617.
[34] Solar district heating, supported by INTELLIGENT ENERGY EUROPE. [Online]. Available: http://www.solar-district-heating.eu/Home.aspx.
[35] C. Peters, D. Serrano, A. Andreu, District heating and cooling from renewable and waste energy in Barcelona. 17th Building Services, Mechanical and Building Industry Days International Conference, 13-14 October 2011, Debrecen, Hungary.
[36] J. Vartiainen, J. Salmi, "District cooling in Helsinki," Helsingin Egergia, 2011. [Online]. Available: http://www.helen.fi/pdf/kj/en/General_Presentation_January_2011.pdf.
[37] S.A. Klein, W.A. Beckman, J.A. Duffie, A design procedure for solar heating systems, Solar Energy 18 (1976) 113-127.
[38] J.D. Balcomb, J.C. Hedstrom, R.D. McFarland, Simulation analysis of passive solar heated buildings—Preliminary results, Solar Energy 19 (1977) 277-282.
[39] D. Johnston, Solar energy systems installed on Chinese-style buildings, Energy and Buildings 39 (2007) 385-392.
[40] M. Castillo-Cagigal, E. Matallanas, D. Masa-Bote, E. Caamano-Martin, A. Gutierrez, F. Monasterio, J. Jimenez-Leube, "Self-consumption enhancement with storage system and demand-side management: GeDELOS-PV system," In 5th International Renewable Energy Storage Conference (IRES 2010), Berlin, Germany, November 22nd-24th.
[41] J. Kurnitski, F. Allard, D. Braham, D. van Dijk,Guillaume Goeders, Jonas Gräslund, et al., "REHVA nZEB technical definition and system boundaries for nearly zero energy buildings, 2013 revision for uniformed national

implementation of EPBD recast prepared in cooperation with European standardization organization CEN," REHVA Federation of European Heating, Ventilation and Air Conditioning Associations, 2013.
[42] PrEN 15603 Energy Performance of Buildings — Overarching standard EPBD (draft), CEN/TC 371, December 2012.
[43] SEL (Solar Energy Laboratory, Univ. of Wisconsin-Madison), TRANSSOLAR (TRANSSOLAR Energietechnik GmbH), CSTB (Centre Scientifique et Technique du Bâtiment), TESS (Thermal Energy Systems Specialists), "TRNSYS 17 A Transient System Simulation Programme Volume 4 Mathematical Reference," the documentations attached in the software package of TRNSYS 17 for the Standard Component Library.
[44] Finland. Ministry of the Environment, Department of the Built Environment, National Building Code of Finland, Part D3, Energy Efficiency in Buildings Regulations and Guidelines 2012 (in Finnish). Directive 2010/31/EC of the European Parliament and of the council (32010L0031); OJ L 153, 18 June 2010, p. 13, DRAFT 28 Sep 2010. [online]. Available: http://www.ymparisto.fi/download.asp?contentid=121170&lan=FI.
[45] China. Ministry of Construction, General Administration of Quality Supervision, Inspection and Quarantine, Design standard for energy efficiency of public buildings GB 50189-2005 (in Chinese). China Architecture and Building Press, 2005.
[46] P.O. Fanger, Thermal Comfort, US: McGraw-Hill Inc.; 1973.
[47] J. Heinonen, J. Kurnitski, T. Tissari, "RET-mallitoimistorakennus energialaskentaan (model calculation of the energy efficient office building)," (in Finnish), HVAC Laboratory, Aalto University School of Engineering, 2005.
[48] Carrier, "AQUAZONE™ 50PSW036-360 Water-to-Water Water Source Heat Pump with PURON® Refrigerant (R410-A) 50 Hz 8.6 to 68.2 Nominal kW," Carrier 50PSW AQUAZONE™, 2011. [Online]. Available: http://www.commercial.carrier.com/commercial/hvac/product_technical_literature/1,3069,CLI1_DIV12_ETI4906_PRD1516,00.html.
[49] "Soil Temperature at Helsinki Tapulikaupunki," Helsinki Weather Information. [Online]. Available: http://www.helsinkiweather.info/soiltemp/.
[50] X.Q. Zhai, Y. Yang, Experience on the application of a ground source heat pump system in an archives building. Energy and Buildings 43 (2011) 3263-3270.
[51] F. Sick, T. Erge, "Photovoltaics in Buildings: A Design Handbook for Architects and Engineers," IEA-SHC Task 16 Publications&Outcomes, 1995. [Online]. Available: http://task16.iea-shc.org/publications.
[52] "Viridian Solar Clearline Solar Thermal Panels," viridiansolar.co.uk. [Online]. Available: http://www.viridiansolar.co.uk/index.htm.
[53] M. Schubert, SOLID, "Solar district heating guidelines, Decentral integration of ST in DH systems," 6.2 Decentralized integration of ST in DH networks, SDH Solar district heating, supported by INTELLIGENT ENERGY EUROPE. [Online]. Available: http://www.solar-district-heating.eu/Documents/SDHGuidelinesDiscussionBoard/62DecentralizedintegrationofSTinDHnetworks.aspx.
[54] "Price list www.solarhome.ru," solarhome.ru, July 11th 2012. [Online]. Available: http://www.solarhome.ru/catalog/price_att.php?language=en.
[55] Whispertech micro-CHP Stirling engine. [Online]. Available: http://www.whispergen.com/
[56] Infinia Corporation. [Online]. Available: http://www.infiniacorp.com
[57] Viessmann Micro-CHP. [Online]. Available: http://www.viessmann.com/com/en/products/Micro_CHP.html
[58] Microgen Engine Corporation. [Online]. Available: http://www.microgen-engine.com
[59] Stirling systems Ltd. [Online]. Available: http://www.stirling-systems.ch
[60] S. Thiers, B. Aoun, B. Peuportier, Experimental characterization, modeling and simulation of a wood pellet micro-combined heat and power unit used as a heat source for a residential building, Energy and Buildings 42 (2010) 896–903.
[61] Cleanergy CHP Engines. [Online]. Available: http://www.cleanergy.com/chp/
[62] The Kingston, Genlec Ltd. [Online]. Available: http://www.genlec.com/products/kingston.html
[63] Micro-Cogeneration, COGEN Microsystems. [Online]. Available: http://www.cogenmicro.com/index.php?select=165
[64] Household Gas Engine Cogenration Unit, Honda Motor Co., Ltd. [Online]. Available: http://world.honda.com/power/cogenerator/
[65] Elcore 2400 PEMFC, Elcore GmbH (in German). [Online]. Available: http://www.elcore2400.com/produkt/technische-daten.html
[66] Hexis SOFC, Hexis AG. [Online]. Available: http://www.hexis.com/en/home
[67] BAXI INNOTECH fuel cell heating. [Online]. Available: http://www.baxi-innotech.de/index.php?id=67&lang=1#c355
[68] Vaillant wall-hung fuel cell heating appliance. [Online]. Available: http://www.vaillant.de/Presse/Press-Releases/article/Vaillant_Group_presents_first_wall-hung_fuel_cells_heating_appliance.html

Attachment of original publications

The challenging EU legislation for nearly zero-energy buildings (nZEB), on one hand, leads to the continuously decreased annual primary energy consumption/equivalent $CO_2$ emission, whereas on the other hand it brings in an inevitable side-effect which is the matching problem between the on-site generation and local building demand. However, the scientific gap is that there is a lack of comprehensive methodology for the matching analysis of the increasingly complicated on-site hybrid energy systems involving all the energy forms, energy conversions, diversified storage types and hybrid grid connections. The purpose of this thesis is to close this gap by developing a comprehensive methodology for evaluating both the general and detailed specific matching situations. This methodology will be greatly beneficial for aiding the analysis, design and control of future on-site nZEB energy systems.

ISBN 978-952-60-5562-6
ISBN 978-952-60-5563-3 (pdf)
ISSN-L 1799-4934
ISSN 1799-4934
ISSN 1799-4942 (pdf)

**Aalto University**
**School of Engineering**
**Department of Energy Technology**
**www.aalto.fi**

BUSINESS + ECONOMY

ART + DESIGN + ARCHITECTURE

SCIENCE + TECHNOLOGY

CROSSOVER

**DOCTORAL DISSERTATIONS**

Aalto-DD 18/2014